From: "Molecular Modeling Theory: Applications in the Geosciences" , R. T. Cygan and J. D. Kubicki., Editors.
Reviews in Mineralogy and Geochemistry, v.42, Mineralogical Society of America, Washington, D.C., 2001, pp. 83-130.

4 Molecular Simulations of Liquid and Supercritical Water: Thermodynamics, Structure, and Hydrogen Bonding

Andrey G. Kalinichev

Department of Geology
University of Illinois at Urbana-Champaign
1301 W. Green St., Urbana, Illinois, 61801, U.S.A.

and

Institute of Experimental Mineralogy
Russian Academy of Sciences
Chernogolovka, Moscow Region, 142432, Russia

INTRODUCTION

Water is a truly unique substance in many respects. It is the only chemical compound that naturally occurs in all three physical states (solid, liquid and vapor) under the thermodynamic conditions typical to the Earth's surface. It plays the principal role in virtually any significant geological and biological processes on our planet. Its outstanding properties as a solvent and its general abundance almost everywhere on the Earth's surface has made it also an integral part of many technological processes since the very beginning of the human civilization.

Aqueous fluids are crucial for the transport and enrichment of ore-forming constituents (Barnes 1997; Planetary Fluids 1990). Quantitative analysis of hydrothermal and metamorphic processes requires information on the physical-chemical, thermodynamic and transport properties of the fluid phases involved (Helgeson 1979, 1981; Sverjensky 1987; Eugster and Baumgartner 1987; Seward and Barnes 1997). These processes encompass a broad range of pressure and temperature conditions and, therefore, detailed understanding of the pressure and temperature dependencies of density, heat capacity, viscosity, diffusivities, and other related properties is necessary in order to develop realistic models of fluid behavior or fluid-mineral interactions.

Aqueous fluids under high-pressure, high-temperature conditions near and above the critical point of water (P = 22.1 MPa and T = 647 K) are especially important in a variety of geochemical processes. Due to the large compressibility of supercritical fluid, small changes in pressure can produce very substantial changes in density, which, in turn, affect diffusivity, viscosity, dielectric, and solvation properties, thus dramatically influencing the kinetics and mechanisms of chemical reactions in water. Models of hydrothermal convection suggest that the near-critical conditions provide an optimal convective behavior due to unique combination of thermodynamic and transport properties in this region of the phase diagram of water (Norton 1984; Jupp and Schultz 2000). Directly measured temperatures of seafloor hydrothermal vents reach near-critical values of 630-680 K, which greatly affects the speciation in these complex chemical systems (Tivey et al. 1990; Von Damm 1990).

From an engineering viewpoint, supercritical water has also attracted growing attention in recent years as a promising chemical medium with a wide range of different environmentally friendly technological applications (Levelt-Sengers 1990; Shaw et al. 1991; Tester et al. 1993). From either geochemical or technological perspective, a fundamental understanding of the complex properties of supercritical aqueous systems

1529-6466/00/0042-0004$05.00

and the ability to reliably predict them using physically meaningful models is of primary importance.

It is a common knowledge that many anomalous properties of water as a solvent arise as a consequence of specific hydrogen bonding interactions of its molecules. Under ambient conditions these anomalous properties of liquid water arise from the competition between nearly ice-like tetrahedrally coordinated local patterns characterized by strong hydrogen bonds and more compact arrangements characterized by more strained and broken bonds (e.g., Stillinger 1980; Okhulkov et al. 1994; Kalinichev et al. 1999). The question of the ranges of temperature and density (or pressure) where these specific interactions can significantly influence the observable properties of water has long been considered very important for the construction of realistic structural models for this fluid (Eisenberg, Kauzmann 1969). The answer to this question varied over time, but as more experimental evidence was gained, the temperature limit for H-bonding in water predicted to be higher and higher. At first, it was thought that hydrogen bonds would disappear above ~420 K. Then, Marchi and Eyring (1964) suggested to shift this limit up to ~523 K, assuming that above this temperature water consists of freely rotating monomers. At the same time, Luck (1965), experimentally studying the IR absorption in liquid water, extended the limit for H-bonding at least up to the critical temperature, 647 K. A subsequent series of high-temperature spectroscopic experiments (Franck and Roth 1967; Bondarenko and Gorbaty 1973, 1991) demonstrated that the upper limit for hydrogen bonds in water had not been reached even at temperatures as high as 823 K. Moreover, x-ray diffraction studies of liquid and supercritical water (Gorbaty and Demianets 1983) gave indications of a non-negligible probability even for tetrahedral configurations of the H-bonded molecules to exist under supercritical conditions of 773 K and 100 MPa.

Direct experimental investigations of the water structure at high temperatures and pressures represent a very challenging undertaking, and any new set of structural or spectroscopic information obtained under such conditions is extremely valuable. Recent introduction into this field of the powerful technique known as neutron diffraction with isotope substitution (NDIS) (Postorino et al. 1993; Bruni et al. 1996; Soper et al. 1997), signified a very important step forward, since this method allows one to experimentally probe all three atom-atom structural correlations in water (OO, OH, and HH) simultaneously. However, it was quite surprising when the very first results of such neutron diffraction measurements were interpreted as the direct evidence of the complete absence of H-bonds in water at near-critical temperatures (Postorino et al. 1993). Despite obvious contradiction with previous experimental data and the results of several molecular computer simulations (Kalinichev 1985, 1986, 1991; Mountain 1989; Cummings et al. 1991), this unexpected conclusion has already made its way into the geochemical literature (Seward and Barnes 1997).

At the same time, amplified by the increasing demand for the detailed molecular understanding of the structure and properties of high-temperature aqueous fluids from the geochemical and engineering communities, this controversy over the degree of hydrogen bonding in supercritical water fuelled a virtual explosion of new experimental and theoretical studies in this field by means of neutron scattering (Soper 1996; Bellisent-Funel et al. 1997; De Jong and Neilson 1997; Botti et al. 1998; Tassaing et al. 1998, 2000; Uffindell et al. 2000), X-ray diffraction (Yamanaka et al. 1994; Gorbaty and Kalinichev 1995), optical spectroscopy (Bennett and Johnston 1994; Bondarenko and Gorbaty 1997; Gorbaty and Gupta 1998; Gorbaty et al. 1999; Hu et al. 2000), NMR spectroscopy (Hoffmann and Conradi 1997; Matubayasi et al. 1997a,b), microwave spectroscopy (Yao and Okada 1998), and computer simulations (Chialvo and Cummings

1994, 1996, 1999; Fois et al. 1994; Kalinichev and Bass 1994, 1995, 1997; Löffler et al. 1994; Mizan et al. 1994, 1996; Cui and Harris 1994, 1995; Duan et al 1995; Mountain 1995, 1999; Kalinichev and Heinzinger 1995; Balbuena et al. 1996a,b; Chialvo et al. 1998, 2000; Driesner et al. 1998; Famulari et al. 1998; Jedlovszky et al. 1998, 1999; Kalinichev and Gorbaty 1998; Liew et al. 1998; Kalinichev and Churakov 1999; Matubayasi et al. 1999; Reagan et al. 1999; Churakov and Kalinichev 2000).

By the early 1990s, classical Monte Carlo (MC) and Molecular Dynamics (MD) computer simulations had already become powerful tools in the studies of the properties of complex molecular liquids, including aqueous solutions (e.g., Heinzinger 1986, 1990). Being neither experiment nor theory, computer "experiments" can, to some extent, take over the task of both in these investigations. The greatest advantage of simulation techniques over conventional theoretical approaches is in the limited number of approximations used. Provided one has a reliable way to calculate inter- and intramolecular potentials, the simulations can lead to information on a wide variety of properties (thermodynamic, structural, transport, spectroscopic, etc.) of the systems under study. In the case of simple fluids, like liquid noble gases, the results of computer simulations have long been used as an "experimental" check against analytical theories (see e.g., Hansen and McDonald 1986). In the case of complex molecular fluids, like aqueous systems over a wide range of temperatures and densities, which still cannot be adequately treated on a molecular level analytically, the computer simulations can play the role of the theory. They can predict thermodynamic, structural, transport, and spectroscopic properties of fluids that can be directly compared with corresponding experimental data. Even more important, however, is the ability of computer simulations to generate and analyze in detail complex spatial and energetic arrangements of every individual water molecule in the system, thus providing extremely useful micro-thermodynamic and micro-structural information not available from any real physical measurement. This gives us a unique tool for better understanding of many crucial correlations between thermodynamic, structural, spectroscopic and transport properties of complex molecular systems on a fundamental atomistic level.

Since the first MC (Barker and Watts 1969) and MD (Rahman and Stillinger 1971) simulations of pure liquid water, great progress has been made in the simulation studies of aqueous systems. One of the earliest significant results was the ruling out of "iceberg" formation in liquid water. Computer simulations—in spite of quite different interatomic potentials employed—have unequivocally shown that liquid water consists of a macroscopically connected, random network of hydrogen bonds continuously undergoing topological reformations (Stillinger 1980). The effects of temperature and pressure on the structure and properties of water and aqueous solutions were also the subject of early computer simulations. However, in most studies either high pressures (Stillinger and Rahman 1974b; Impey et al. 1981; Jancsó et al. 1984; Pálinkás et al. 1984; Madura et al. 1988) or high temperatures (Stillinger and Rahman 1972, 1974a; Jorgensen and Madura 1985; De Pablo and Prausnitz 1989) were applied to the system, and the range of temperatures was usually well below the critical temperature of water.

Surprisingly, the first molecular computer simulation of supercritical steam (Beshinske and Lietzke 1969) was published almost simultaneously with the first ever MC simulation of liquid water (Barker and Watts 1969). However, until the last decade, molecular simulations of supercritical aqueous fluids remained relatively scarce (O'Shea and Tremaine 1980; Kalinichev 1985, 1986, 1991; Kataoka 1987, 1989; Evans et al. 1988; Mountain 1989; De Pablo et al. 1989, 1990; Cummings et al. 1991). Several reviews have already been published which summarize the state of this field of research by the early 1990s (Heinzinger 1990; Belonoshko and Saxena 1992; Fraser and Refson

1992; Kalinichev and Heinzinger 1992).

The aim of this chapter is to provide an overview of the most recent results obtained by the application of computer simulation techniques to the studies of various microscopic and macroscopic properties of supercritical water over a range of densities relevant to geochemical applications and varying about two orders of magnitude from relatively dilute vapor-like to highly compressed liquid-like fluids. The general simulation methodology will be briefly described first, followed by the discussion of interaction potentials most frequently used in high-temperature and high-pressure aqueous simulations. The thermodynamics and structure of supercritical water are further discussed in relation to a detailed analysis of hydrogen bonding statistics in supercritical water based on the proposed hybrid geometric and energetic criterion of H-bonding and intermolecular distance-energy distribution functions (Kalinichev and Bass 1994). We show that after the initial interpretation of the first supercritical neutron diffraction results (Postorino et al. 1993) was eventually corrected (Soper et al. 1997), very good consistency now exists between several independent sources of experimental data and numerous computer simulation results, which all indicate that a significant degree of hydrogen bonding still persists in water under supercritical conditions. The dynamics of translational, librational, and intramolecular vibrational motions of individual molecules in supercritical water will be discussed in the last section. A more detailed discussion of the controversy associated with the contradictions between the initial NDIS measurements and molecular-based modeling of the structure and thermodynamics of supercritical aqueous solutions, in many ways complementary to the present chapter, the reader can find in the excellent recent review by Chialvo and Cummings (1999).

CLASSICAL METHODS OF MOLECULAR SIMULATIONS

Two sets of methods for computer simulations of molecular fluids have been developed: Monte Carlo (MC) and Molecular Dynamics (MD). In both cases the simulations are performed on a relatively small number of particles (atoms, ions, and/or molecules) of the order of $100 < N < 10{,}000$ confined in a periodic box, or simulation supercell. The interparticle interactions are represented by pair potentials, and it is generally assumed that the total potential energy of the system can be described as a sum of these pair interactions. Very large numbers of particle configurations are generated on a computer in both methods, and, with the help of statistical mechanics, many useful thermodynamic and structural properties of the fluid (pressure, temperature, internal energy, heat capacity, radial distribution functions, etc.) can then be directly calculated from this microscopic information about instantaneous atomic positions and velocities.

Many good textbooks and monographs introducing and discussing theoretical fundamentals of statistical physics and molecular computer simulations of fluid systems are available in the literature (e.g., McQuarrie 1976; Hansen and McDonald 1986; Allen and Tildesley 1987; Frenkel and Smit 1996; Robinson et al. 1996; Balbuena and Seminario 1999). Therefore, we only briefly mention here for completeness the most basic concepts and relationships.

Molecular dynamics

In MD simulations, the classical Newtonian equations of motion are numerically integrated for all particles in the simulation box. The size of the time step for integration depends on a number of factors, including temperature and density, masses of the particles and the nature of the interparticle potential, and the general numeric stability of the integration algorithm. In the MD simulations of aqueous systems, the time step is typically of the order of femtoseconds (10^{-15} s), and the dynamic trajectories of the

molecules are usually followed (after a thermodynamic pre-equilibration) for 10^4 to 10^6 steps, depending on the properties of interest.

The resulting knowledge of the trajectories for each of the particles (i.e., particle positions, velocities, as well as orientations and angular velocities if molecules are involved) means a complete description of the system in a classical mechanical sense. The thermodynamic properties of the system can then be calculated from the corresponding time averages. For example, the temperature is related to the average value of the kinetic energy of all molecules in the system:

$$T = \frac{2}{3Nk_{\mathrm{B}}} \left\langle \sum_{i=1}^{N} \frac{m_i \mathbf{v}_i^2}{2} \right\rangle \tag{1}$$

where m_i and $\mathbf{v}_i$ are the masses and the velocities of the molecules in the system, respectively.

Pressure can be calculated from the virial theorem:

$$P = \frac{Nk_{\mathrm{B}}T}{V} - \left(\frac{1}{3V} \right) \left\langle \sum_{i=1}^{N} \mathbf{r}_i \cdot \mathbf{F}_i \right\rangle \tag{2}$$

where V is the volume of the simulation box and $(\mathbf{r}_i \cdot \mathbf{F}_i)$ means the dot product of the position and the force vectors of particle i.

The heat capacity of the system can be calculated from temperature fluctuations:

$$C_V = R \left(\frac{2}{3} - N \frac{\left\langle T^2 \right\rangle - \left\langle T \right\rangle^2}{\left\langle T \right\rangle^2} \right)^{-1} \tag{3}$$

where R is the gas constant. In the Equations (1)–(3), k_{B} is the Boltzmann constant, and angular brackets denote the time-averaging along the dynamic trajectory of the system.

Molecular dynamics simulations may be performed under a variety of conditions and constraints, corresponding to different *ensembles* in statistical mechanics. Most commonly the *microcanonical* (*NVE*) ensemble is used, i.e., the number of particles, the volume, and the total energy of the system remain constant during the simulation. The relationships in Equations (1)–(3) are valid for this case.

There are several modifications of the MD algorithm, allowing one to carry out the simulations in the *canonical* (*NVT*) or *isothermal-isobaric* (*NPT*) ensembles. Relationships similar to Equations (1)–(3) and many others can be systematically derived for these ensembles, as well (Allen and Tildesley 1987; Frenkel and Smit 1996).

Monte Carlo methods

In MC simulations, a large number of thermodynamically equilibrium particle configurations are created on a computer using a random number generator by the following scheme. Starting from a given (almost arbitrary) configuration, a trial move of a randomly (or cyclically) chosen particle to a new position—as well as to a new orientation if rigid molecules are involved—is attempted. The potential energy difference, ΔU, associated with this move is then calculated, and if $\Delta U \leq 0$, the new configuration is unconditionally accepted. However, if $\Delta U > 0$, the new configuration is not rejected outright, but the Boltzmann factor $\exp(-\Delta U/k_{\mathrm{B}}T)$ is first calculated and compared with a randomly chosen number between 0 and 1. The move is accepted if the Boltzmann factor is larger than this number, and rejected otherwise. In other words, the

trial configuration is accepted with the following probability:

$$p = \begin{cases} 1, & \Delta U \le 0 \\ \exp(-\Delta U / k_B T) & \Delta U > 0 \end{cases} \quad (4)$$

Reiteration of such a procedure gives a *Markov chain* of molecular configurations distributed in the phase space of the system, with the probability density proportional to the Boltzmann weight factor corresponding to the canonical *NVT* statistical ensemble.

Typically, about 10^6 configurations are generated after some pre-equilibration stage of about the same length. The thermodynamic properties of the system can then be calculated as the averages over the ensemble of configurations. The equivalence of ensemble- and time-averages, the so-called *ergodic hypothesis*, constitutes the basis of statistical mechanics (e.g., McQuarrie 1976).

The ranges of maximum molecular displacement and rotation are usually adjusted during the pre-equilibration stage for each run to yield an acceptance ratio of about 0.5. If these ranges are too small or too large, the acceptance ratio becomes closer to 1 or 0, respectively, and the phase space of the system is explored less efficiently.

The advantage of the MC method is that it can be more readily adapted to the calculation of averages in any statistical ensemble (Allen and Tildesley 1987; Frenkel and Smit 1996). For example, to perform simulations in the *NPT* ensemble, one can introduce volume-changing trial moves. All intermolecular distances are then scaled to a new box size. The acceptance criterion is then also changed accordingly. Instead of the energy difference ΔU in Equation (4), one should now use the enthalpy difference

$$\Delta H = \Delta U + P\Delta V - k_B T \ln(1 + \Delta V/V)^N \quad (5)$$

where P is the pressure (which is kept constant in this case) and V is the volume of the system.

In this ensemble, besides the trivial averages for configurational (i.e., due to the intermolecular interactions) enthalpy:

$$H_{conf} = \langle U \rangle + P\langle V \rangle \quad (6)$$

and molar volume:

$$V_m = \langle V \rangle N_A / N \quad (7)$$

such useful thermodynamic properties as isobaric heat capacity C_P, isothermal compressibility κ, and thermal expansivity α can be easily calculated from the corresponding fluctuation relationships (e.g., Landau and Lifshitz 1980):

$$C_P = \left(\frac{\langle H^2 \rangle - \langle H \rangle^2}{N k_B T^2} \right) \quad (8)$$

$$\kappa \equiv -\frac{1}{V}\left(\frac{\partial V}{\partial P} \right)_T = \left(\frac{\langle V^2 \rangle - \langle V \rangle^2}{N k_B T \langle V \rangle} \right) \quad (9)$$

$$\alpha \equiv \frac{1}{V}\left(\frac{\partial V}{\partial T}\right)_P = \left(\frac{\langle H_{\text{conf}} V\rangle - \langle H_{\text{conf}}\rangle\langle V\rangle}{Nk_{\text{B}}T^2\langle V\rangle}\right) \tag{10}$$

The *grand canonical* (μVT) statistical ensemble, in which the chemical potential of the particles is fixed and the number of particles may fluctuate, is very attractive for simulations of geochemical fluids. So far, however, it has only been barely tested even for pure liquid water simulations (Shelley and Patey 1995; Lynch and Pettitt 1997; Shroll and Smith 1999a,b). At the same time, the technique of *Gibbs ensemble* Monte Carlo simulation (Panagiotopoulos 1987), which permits direct calculations of the phase coexistence properties of pure components and mixtures from a single simulation, was introduced and successfully used for calculations of the vapor-liquid coexistence properties of water (De Pablo and Prausnitz 1989; De Pablo et al. 1990; Kiyohara et al. 1998; Errington and Panagiotopoulos 1998; Panagiotopoulos 2000).

Molecular dynamics simulations have generally a great advantage of allowing the study of time-dependent phenomena. However, if thermodynamic and structural properties alone are of interest, Monte Carlo methods might be more useful. On the other hand, with the availability of ready-to-use computer simulation packages (e.g., Molecular Simulations Inc. 1999), the implementation of particular statistical ensembles in molecular dynamics simulations becomes nowadays much less problematic even for an end user without deep knowledge of statistical mechanics.

Boundary conditions, long-range corrections, and statistical errors

One of the most obvious difficulties arises in both simulation methods from the relatively small system size, always much smaller than the Avogadro number, N_{A}, characteristic for a macroscopic system. Therefore, so-called *periodic boundary conditions* are usually applied to the simulated system in order to minimize surface effects and to simulate more closely its bulk macroscopic properties. This means that the basic simulation box is assumed to be surrounded by identical boxes in all three dimensions infinitely. Thus, if a particle leaves the box through one side, its image enters simultaneously through the opposite side, because of the identity of the boxes. In this way, the problem of surfaces is circumvented at the expense of the introduction of periodicity.

Whether the properties of a small infinitely periodic system and the macroscopic system, which the model is designed to represent, are the same, depends on the range of the intermolecular potential and the property under investigation. For short-range interactions, either spherical or minimum image cutoff criteria are commonly used (Allen and Tildesley 1987; Frenkel and Smit 1996). The latter means that each molecule interacts only with the closest image of every other molecule in the basic simulation box or in its periodic replica. However, any realistic potential for water (not to mention electrolyte solutions) contains long-range Coulomb interactions, which should be properly taken into account. Several methods to treat these long-range interactions are commonly used (see, e.g., Allen and Tildesley 1987), of which the *Ewald summation* is usually considered as the most satisfactory one. (See the discussion Gale, this volume).

As any experimental method, computer simulations may also be subject to statistical errors. Since all simulation averages are taken over MD or MC runs of finite length, it is essential to estimate the statistical significance of the results. The statistical uncertainties of simulated properties are usually estimated by the method of block averages (Allen and Tildesley 1987). The MD trajectory or the MC chain of molecular configurations is subdivided into several non-overlapping blocks of equal length, and the averages of every

property are computed for each block. If $\langle A \rangle_i$ is the mean value of the property A computed over the block i, then the statistical error δA of the mean value $\langle A \rangle$ over the whole chain of configurations can be estimated as

$$(\partial A)^2 = \frac{1}{M(M-1)} \sum_{i=1}^{M} \left[\left\langle A^2 \right\rangle_i - \left\langle A \right\rangle_i^2 \right] \tag{11}$$

where M is the number of blocks.

Strictly speaking, Equation (11) is only valid if all $\langle A \rangle_i$ are statistically independent and show a normal Gaussian distribution. Thus, in computer simulations of insufficient length, these error bound estimates should be taken with caution, especially for the properties calculated from fluctuations, such as Equations (3), (8)–(10). The analysis of convergence profiles of the running averages for the simulated properties is very useful in this case. One can roughly estimate the limits of statistical errors as maximum variations of the running averages during the final equilibrium stage of the simulation.

Interaction potentials for aqueous simulations

Interactions between water molecules are far more complicated than those between particles of simple liquids. This complexity displays itself in the ability of H_2O molecules to form hydrogen bonds, making water an associated liquid. An additional difficulty in the description of water-water interactions is the existence of substantial non-additive three- and higher-body terms, studied in detail by several authors (Gellatly et al. 1983; Clementi 1985; Gil-Adalid 1991; Famulari et al. 1998), which may raise doubts on the applicability of the pair-additivity approximation ordinarily used in computer simulations.

On the other hand, the analysis of experimental shockwave data for water has shown (Ree 1982) that at the limit of high temperatures and pressures intermolecular interactions of water become simpler. In this case, it becomes even possible to use a spherically-symmetric model potential for the calculations of water properties either from computer simulations (Belonoshko and Saxena 1991, 1992) or from thermodynamic perturbation theory in a way similar to simple liquids (Hansen and McDonald 1986). However, such simplifications exclude the possibility of understanding many important and complex phenomena in aqueous fluids on a true molecular level, which is, actually, the strongest advantage and the main objective of molecular computer simulations.

The pair potential functions for the description of the intermolecular interactions used in molecular simulations of aqueous systems can be grouped into two broad classes as far as their origin is concerned: empirical and quantum mechanical potentials. In the first case, all parameters of a model are adjusted to fit experimental data for water from different sources, and thus necessarily incorporate effects of many-body interactions in some implicit average way. The second class of potentials, obtained from *ab initio* quantum mechanical calculations, represent purely the pair energy of the water dimer and they do not take into account any many-body effects. However, such potentials can be regarded as the first term in a systematic many-body expansion of the total quantum mechanical potential (Clementi 1985; Famulari et al. 1998; Stern et al. 1999).

In the last two decades both types of potentials have been extensively used in computer simulations of aqueous systems. Several studies comparing the abilities of different potentials for reproducing a wide range of gas-phase, liquid, and solid state properties of water are currently available (Reimers et al. 1982; Morse and Rice 1982; Jorgensen et al. 1983; Clementi 1985; Robinson et al. 1996; Jorgensen and Jenson 1998; Kiyohara et al. 1998; Van der Spoel et al. 1998; Balbuena et al. 1999; Floris and Tani

1999; Jedlovszky and Richardi 1999; Wallqvist and Mountain 1999; Panagiotopoulos 2000). These comparisons have shown that none of the models is able to give a satisfactory account of all three phases of water simultaneously. On the other hand, they demonstrated that many properties of aqueous systems can be qualitatively and even quantitatively reproduced in computer simulations irrespective of the interaction potential used, thus verifying the reliability of the models.

Typical structures of empirical water models are schematically shown in Figure 1. Historically, the very first MD simulations of water at high pressure were performed with the empirical ST2 model (Stillinger and Rahman 1974b). It is a 5-point rigid model with four charges arranged tetrahedrally around the oxygen atom (Fig. 1c). The positive charges are located at the hydrogen atoms at a distance of 1 Å from the oxygen atom, nearly the real distance in the water molecule. The negative charges are located at the other two vertices of the tetrahedron (sites t1 and t2 in Fig. 1) but at a distance of only 0.8 Å from the oxygen. The charges were chosen to be 0.23*e* leading to roughly the correct dipole moment of the water molecule. The tetrahedrally arranged point charges render possible the formation of hydrogen bonds in the right directions. The ST2 model is completed by adding a (12-6) Lennard-Jones (LJ) potential, the center of which is located at the oxygen atom, with $\sigma = 3.10$ Å and $\varepsilon = 0.317$ kJ/mol. The total interaction energy for a pair of molecules i and j consists of the Coulomb interactions between all the charged sites and the Lennard-Jones interaction between the oxygen atoms:

$$U_{ij}(r) = \sum_{\alpha,\beta} \frac{q_\alpha q_\beta}{r_{\alpha\beta}} + 4\varepsilon\left[\left(\frac{\sigma}{r_{OO}}\right)^{12} - \left(\frac{\sigma}{r_{OO}}\right)^{6}\right] \tag{12}$$

where α and β are indices of the charged sites. A special switching function was added to the Coulomb term of this water pair potential in order to reduce unrealistic Coulomb forces between very close water molecules.

This ST2 model was employed in the earlier series of MD simulations of aqueous alkali halide solutions (Heinzinger and Vogel 1976). Evans (1986) later proposed a modification of the ST2 potential which included atom-atom LJ terms centered both on the oxygen and hydrogen atoms, thus eliminating the need to use the switching function. This model has been employed in MD simulations of water at temperatures up to 1273 K and at constant densities of 1.0 and 0.47 g/cm^3 (Evans et al. 1988) and has shown, within the statistical uncertainty, a satisfactory reproducibility of the experimental pressure in this range and at the critical point of water.

Another empirical water model often used in simulations at supercritical conditions

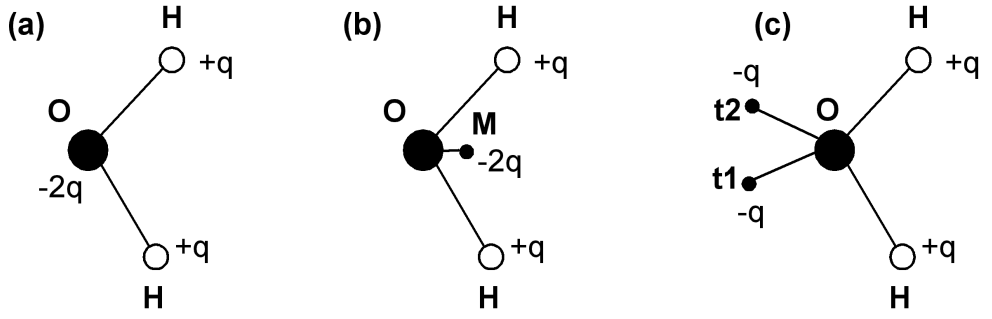

Figure 1. Schematic diagrams of (a) 3-point, (b) 4-point, and (c) 5-point models of a water molecule.

is the TIP4P model (Jorgensen et al. 1983). It differs from the ST2 model in several aspects. The rigid geometry employed is that of the gas phase monomer with an OH distance of 0.9572 Å and an HOH angle of 104.52°. The two negative charges are reduced to a single one at a point M positioned on the bisector of the HOH angle at a distance of 0.15 Å in direction of the H atoms (Fig. 1b), which bear a charge of +0.52*e*. This simplification of the charge distribution also improves the performance of the model, since it is known that the negative charges in the tetrahedral vertices of the ST2 model exaggerate the directionality of the lone pair orbitals of the water molecule and the degree of hydrogen bonding exhibited by this model. On the other hand, Mahoney and Jorgensen (2000) have recently introduced a 5-point TIP5P model, specifically designed to accurately reproduce the density anomaly of water near 4°C. So far, this model has only been tested at temperatures below 100°C, and its behavior at supercritical temperatures is not yet known.

In the TIP4P model there is a (12-6) Lennard-Jones term centered at the oxygen atom with the parameters $\sigma = 3.1536$ Å and $\varepsilon = 0.649$ kJ/mol. This larger value for ε compared with the ST2 and TIP5P models compensates for the reduction in Coulomb energy because of the fact that the opposite charges cannot approach as near as in a 5-point model.

The TIP4P water model has already proved its reliability in numerous molecular simulations of various water properties over wide ranges of temperatures and pressures (densities). The TIP4P model was widely used in the investigations of thermodynamics, structure and hydrogen bonding in supercritical water (Mountain 1989; and Kalinichev 1991, 1992; Kalinichev and Bass 1994, 1995, 1997; Churakov and Kalinichev 2000) and aqueous solutions (Brodholt and Wood 1993b; Gao 1994; Destrigneville et al. 1996). Thermodynamic and structural properties of TIP4P water at normal temperature and pressures up to 1 GPa (Madura et al. 1988; Kalinichev et al. 1999) as well as at normal density and temperatures up to 2300 K (Brodholt and Wood 1990) have also been studied.

Dielectric properties for this water model have been simulated by Neumann (1986) and Alper and Levy (1989). Motakabbir and Berkowitz (1991) and Karim and Haymet (1988) have simulated vapor/liquid and ice/liquid interfaces, respectively. De Pablo and Prausnitz (1989) and Vlot et al. (1999) have studied vapor-liquid equilibrium properties of the TIP4P model, and have shown that it overestimates the vapor pressure and underestimates the critical temperature of water.

The empirical simple point-charge (SPC) model (Berendsen et al. 1981) and its SPC/E modification (Berendsen et al. 1987) have been most extensively used in molecular modeling of aqueous systems over the last two decades. This is a 3-site model (Fig. 1a) with partial charges located directly on the oxygen and hydrogen atoms. The SPC and SPC/E models have a rigid geometry and LJ parameters quite similar to those of the TIP4P model. Flexible versions of the SPC model have also been introduced (Toukan and Rahman 1985; Dang and Pettitt 1987; Teleman et al. 1987). Guissani et al. (1988) made the first attempt to calculate the *p*H value of water from MD simulations and, after all polarization effects included, achieved a rather good agreement with experiment up to 593 K. The calculated static dielectric constant of the SPC/E water model is in good quantitative agreement with experiment over a very wide range of temperatures and densities (Wasserman et al. 1995), which is important for realistic simulations of the properties of supercritical aqueous solutions of electrolytes (Balbuena et al. 1996a,b; Cui and Harris 1994, 1995; Re and Laria 1997; Brodholt 1998; Driesner et al. 1998; Reagan et al. 1999) and non-electrolytes (Lin and Wood 1996).

The SPC model was successfully used in the simulations of the liquid-vapor coexistence curve (De Pablo et al. 1990; Guissani and Guillot 1993; Errington and Panagiotopoulos 1998; Kiyohara et al. 1998). It is able to correctly reproduce vapor pressure, but, like the TIP4P model, underestimates the critical temperature of water. On the other hand, the SPC/E model accurately predicts the critical temperature, but underestimates the vapor pressure by more than a factor of two.

The recently proposed Exp-6 water model uses a more realistic exponential functional form for the repulsive interaction in Equation (12), and was specifically parameterized to reproduce the vapor-liquid phase coexistence properties (Errington and Panagiotopoulos 1998). However, it does not do as well as the TIP4P, SPC, and SPC/E models for the structure of liquid water, especially in terms of the oxygen-oxygen pair correlation function (Panagiotopoulos 2000).

Thus, none of the available fixed point charge models can quantitatively reproduce thermodynamic and structural properties of water over a broad range of temperatures and pressures. It is clear that for strongly interacting molecules, such as H_2O, a simple two-body effective potential is not sufficient, and inclusion of additional interaction terms is necessary. The most important addition is likely to be an explicit incorporation of molecular polarizability. Several polarizable models for water are available in the literature (see, e.g., Robinson et al. 1996; Wallqvist and Mountain 1999 for a review). These models seem to be slightly superior over the fixed point charge models in the description of water structure, but none of them improves the description of the vapor-liquid coexistence properties and critical parameters (Kiyohara et al. 1998; Chen et al. 1999; Chialvo et al. 2000; Jedlovszky et al. 2000). It is important to keep in mind that even with recent methodological developments (Martin et al. 1998; Chen et al. 2000) the explicit incorporation of polarizability in Monte Carlo calculations comes with a penalty of a factor of ten in CPU time relative to calculations with non-polarizable models (Panagiotopoulos 2000).

There are also developed a number of empirical water-water potentials with fixed charges, but incorporating intramolecular flexibility (e.g., Bopp et al. 1983; Toukan and Rahman 1985; Teleman et al. 1987; Barrat and McDonald 1990; Wallqvist and Teleman 1991; Zhu et al. 1991; Corongiu 1992; Smith and Haymet 1992; Halley et al. 1993) since Stillinger and Rahman (1978) first introduced their central force (CF) model. Although incorporation of the molecular flexibility has apparently only minor effect on the thermodynamic and structural properties of simulated water, flexible models have the great advantage of permitting the investigation of the effects of temperature, pressure, and local molecular or ionic environment on the intramolecular properties of water, like molecular geometry, dipole moments, and modes of vibration. Thus, the application of such models in molecular simulations of high-temperature aqueous systems could be particularly helpful in interpretation of some geochemical data, where vibrational spectroscopic techniques are often used as *in situ* probes of the chemical composition, structural speciation, etc. (e.g., Frantz et al. 1993; Bondarenko and Gorbaty 1997; Gorbaty and Gupta 1998; Gorbaty et al. 1999; Hu et al. 2000).

The original CF flexible model of Stillinger and Rahman (1978) consisted of only oxygen and hydrogen atomic sites, bearing partial charges. The correct geometry of a water molecule was solely preserved by an appropriate set of oxygen-hydrogen and hydrogen-hydrogen pair potentials having a rather elaborate functional form. In order to improve the description of the gas-liquid vibrational frequency shifts by the CF model, its modification, known as the BJH water model, was later introduced by Bopp et al. (1983). The total potential is now separated into an *inter*molecular and an *intra*molecular part. The intermolecular pair potential remained only slightly modified version of the CF

model, and is given by:

$$U_{OO}(r) = \frac{604.6}{r} + \frac{111889}{r^{8.86}} - 1.045\left\{\exp\left[-4(r-3.4)^2\right] - \exp\left[-1.5(r-4.5)^2\right]\right\} \quad (13)$$

$$U_{OH}(r) = -\frac{302.2}{r} + \frac{26.07}{r^{9.2}} - \left\{\frac{41.79}{1+\exp\left[40(r-1.05)\right]}\right\} - \left\{\frac{16.74}{1+\exp\left[5.493(r-2.2)\right]}\right\} \quad (14)$$

$$U_{HH}(r) = \frac{151.1}{r} + \left\{\frac{418.33}{1+\exp\left[29.9(r-1.968)\right]}\right\} \quad (15)$$

where energies are in kJ/mol and distances in Å. The first terms in these equations are due to the Coulomb interactions of the partial charges on O and H atoms.

The intramolecular part of the BJH model is based on the formulation of Carney et al. (1976)

$$U_{\text{intra}} = \sum L_{ij}\rho_i\rho_j + \sum L_{ijk}\rho_i \quad (16)$$

with $\rho_1 = (r_1 - r_e)/r_1$, $\rho_2 = (r_2 - r_e)/r_2$, $\rho_3 = \alpha - \alpha_e = \Delta\alpha$, where r_1, r_2 and α are the instantaneous OH bond lengths and HOH angle; the quantities r_e=0.9572Å and α_e=104.52° are their corresponding equilibrium values (Eisenberg and Kauzmann 1969). The intramolecular parameters of the BJH potential are given in Table 1. This model is quite successful in correctly reproducing vibrational spectra of supercritical water (Kalinichev and Heinzinger 1992, 1995) and in the description and interpretation of the temperature and density dependence of ionic hydration in aqueous $SrCl_2$ solutions obtained by EXAFS measurements (Seward et al. 1999; Driesner and Cummings 1999). This model has also performed well in reproducing the dielectric properties of water at ambient and elevated temperatures (Ruff and Diestler 1990; Trokhymchuk et al. 1993). The spectroscopic properties of isotopically substituted BJH water have also been studied (Lu et al. 1996).

From the family of quantum mechanical water potentials, the MCY model (Matsuoka et al. 1976) should be mentioned in the context of high-temperature simulations. This model has the 4-point geometry (Fig. 1b), but a much more complicated functional form with parameters derived from *ab initio* quantum chemical calculations. The flexible version for this model (MCYL) has also been developed (Lie and Clementi 1986). The MCY model was used by Impey et al. (1981) in their MD studies of the structure of water at elevated temperatures and high density, and by O'Shea and Tremaine (1980) in the MC simulations of thermodynamic properties of supercritical water. It is well known, however, that this potential reproduces poorly the pressure at a given density (or the density at a given pressure). Even the

Table 1. Potential constants used for the intramolecular part of the BJH water model in units of kJ/mol (Bopp et al. 1983). The notations are according to Equation (16).

$\rho_1\rho_2(\rho_1+\rho_2)$	-55.7272
$(\rho_1^2 + \rho_2^2)\Delta\alpha$	237.696
$(\rho_1^4 + \rho_2^4)$	5383.67
$\rho_1\rho_2(\rho_1^2 + \rho_2^2)$	-55.7272
$(\rho_1^3 + \rho_2^3)\Delta\alpha$	349.151
$(\rho_1^2 + \rho_2^2)$	2332.27
$\rho_1\rho_2$	-55.7272
$(\rho_1 + \rho_2)\Delta\alpha$	126.242
$(\Delta\alpha)^2$	209.860
$(\rho_1^3 + \rho_2^3)$	-4522.52

addition of quantum mechanical three- and four-body terms to the potential, though extremely demanding in terms of computer time, did not improve the situation significantly (Clementi 1985). A similar *ab initio* CC potential (Carravetta and Clementi 1984) has been used by Kataoka (1987 1989) in extensive MD simulations of thermodynamic and transport properties of fluid water over a wide range of thermodynamic conditions, including supercritical. A qualitative reproduction of anomalous behavior of these properties has been achieved. This approach has been continued by Famulari et al. (1998). A different approach to the parameterization of the "fluctuating-charge" polarizable models from *ab initio* quantum chemical calculations has been recently proposed by Stern et al. (1999).

However, despite of the great importance of quantum mechanical potentials from the purely theoretical point of view, simple effective two-body potential functions for water seem at present to be preferable for the extensive simulations of complex aqueous systems of geochemical interest. A very promising and powerful method of Car-Parrinello *ab initio* molecular dynamics, which completely eliminates the need for a potential interaction model in MD simulations (e.g., Fois et al. 1994; Tukerman et al. 1995, 1997) still remains computationally extremely demanding and limited to relatively small systems ($N < 100$ and a total simulation time of a few picoseconds), which also presently limits its application for complex geochemical fluids. On the other hand, it may soon become a method of choice, if the current exponential growth of supercomputing power will continue in the near future.

THERMODYNAMICS OF SUPERCRITICAL AQUEOUS SYSTEMS

The results of isothermal-isobaric MC simulations discussed in this and the following sections were obtained for a system of N=216 H_2O molecules interacting via the TIP4P potential (Jorgensen et al. 1983) in a cubic cell with periodic boundary conditions. The technical details of the *NPT*-ensemble algorithm are described in detail elsewhere (Kalinichev 1991, 1992). More than 40 thermodynamic states were simulated covering temperatures between 273 and 1273 K over a pressure range from 0.1 to 10000 MPa, thus sampling a very wide density range between 0.02 and 1.67 g/cm^3. For each thermodynamic state point the properties were averaged over 10^7 equilibrium MC configurations with another 5×10^6 configurations generated and rejected on the pre-equilibration stage. The convergence of all the properties was carefully monitored during each simulation run and the statistical uncertainties were calculated by averaging over 50 smaller parts of the total chain of configurations.

The MD simulations discussed in the following sections were performed using a conventional molecular dynamics algorithm for the canonical (*NVE*) ensemble and the flexible BJH water model (Bopp et al. 1983). The systems studied consisted of 200 H_2O molecules in a cubic box with the side length adjusted to give the required density. The densities between 0.17 and 1.28 g/cm^3 were chosen to correspond to the pressure range of $25<P<3000$ MPa.

Each simulation extended to about 15000 time-steps after a pre-equilibration of approximately the same length. Ewald summation in tabulated form was used for the Coulomb interactions, and the "shifted-force" method (e.g., Allen and Tildesley 1987) was used for the non-Coulomb parts of the BJH potential. All technical details of the simulations are described in detail elsewhere (Kalinichev and Heinzinger 1992, 1995; Kalinichev 1993).

Macroscopic thermodynamic properties of simulated supercritical water

In Figure 2 the thermodynamic results of our MC simulations (symbols) are compared with available experimental data (lines). The calculated values of density and configurational enthalpy, H_{config}, isobaric heat capacity, C_P, isothermal compressibility, κ, and thermal expansivity, α, are in excellent agreement with isotherms calculated using the equation of state of Saul and Wagner (1989), which accurately reproduces all available experimental data in this range of thermodynamic parameters. For comparison with experimental data, the non-configurational contributions to the internal energy,

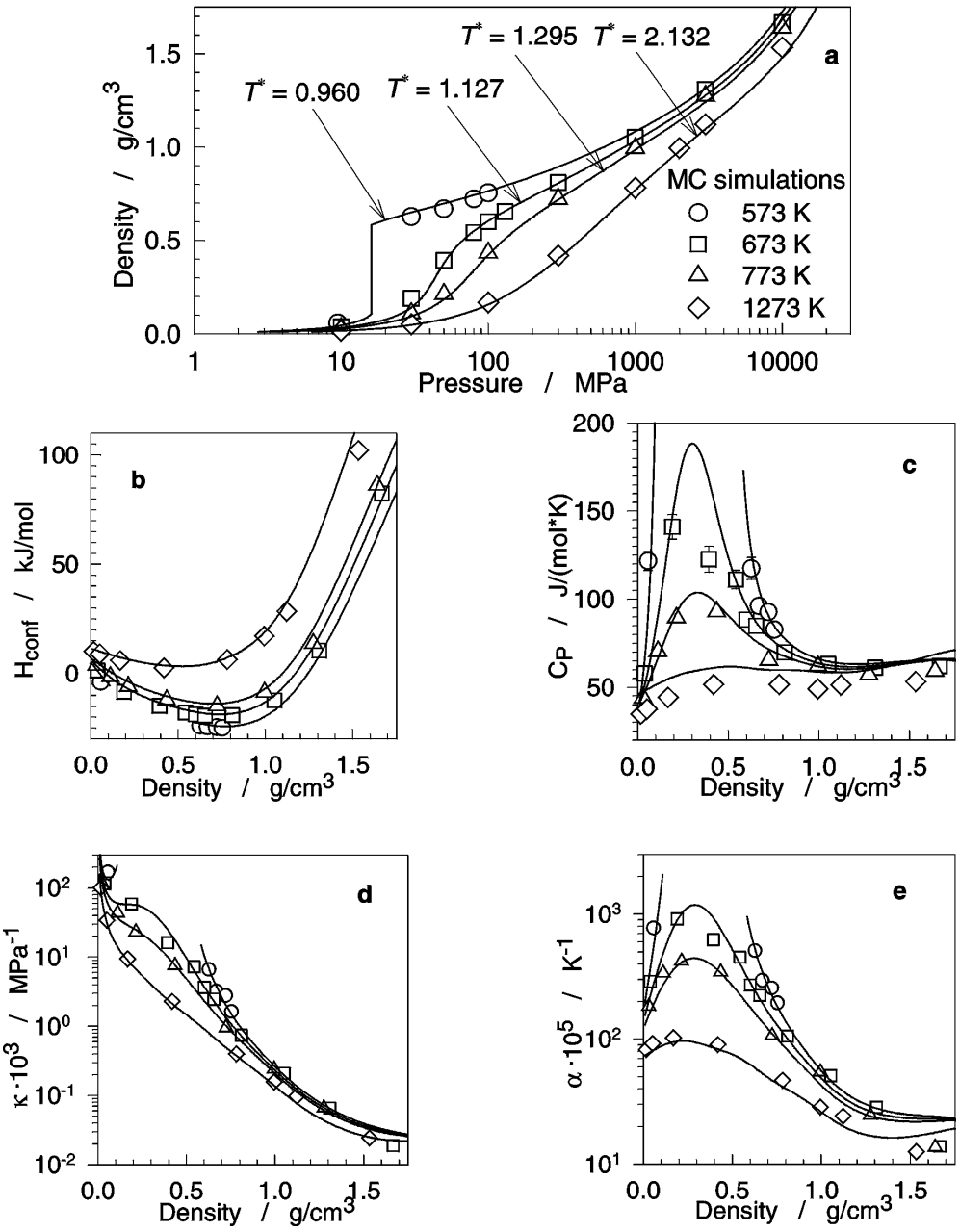

Figure 2. Thermodynamic properties of supercritical water simulated using the TIP4P potential. Symbols are MC results, lines are calculated from the standard equation of state for water (Saul and Wagner 1989).

enthalpy, and heat capacity of supercritical water were assumed to be identical with those for the real gas in its standard state (Woolley 1980). The experimental configurational properties were estimated from the equation of state by

$$U_{\text{conf}} = U(T,V) - U_{\text{i.g.}}(T) \tag{17}$$

and

$$H_{\text{conf}} = H(T,P) - H_{\text{i.g.}}(T) \tag{18}$$

with the ideal gas reference state at the given temperature. No other corrections were added to any property reported. However, since the critical point for the TIP4P water model is lower than observed experimentally (De Pablo et al. 1990; Kalinichev 1991; Vlot et al. 1999), the isotherms in Fig. 2 were scaled in order to represent the same reduced temperature, $T^* = T/T_{\text{c}}$, which is especially important in the near-critical region. The corresponding values of T^* are indicated in Figure 2a for each isotherm.

With this correction, a very realistic representation of many thermodynamic properties of water over extremely wide ranges of temperature and density is observed in molecular computer simulations. This result gives us sufficient confidence in the following quantitative analysis and interpretation of the details of local geometric and energetic environments experienced by individual water molecules in terms of hydrogen bonding under supercritical conditions.

Micro-thermodynamic properties

Atomistic computer simulations are unique in providing a vast amount of detailed thermodynamic information on the properties, which are not readily measured in any experiment. One such property is the bonding energy:

$$E_{\text{b},i} = \sum_{j \neq i}^{N} U_{ij} \tag{19}$$

which reflects the energetic environment experienced by a single water molecule.

Bonding energy distributions. Bonding energy distributions are shown in Figure 3a–d for several typical near- and supercritical thermodynamic states of water. Despite the difference in the potential models used in the MC and MD simulations, they resulted in virtually the same bonding energy distributions when the thermodynamic conditions of the simulations are the same (Kalinichev and Heinzinger 1992). The effect of pressure (or density) changes along the isotherms 573, 673, 773, and 1273 K is clearly seen in Figure 3 for these distributions. As in the case of normal temperature (Madura et al. 1988; Mahoney and Jorgensen 2000), the maxima of the distributions shift to more negative energies and their widths increase with increasing pressure.

It is interesting to note that under supercritical conditions a certain number of molecules even have positive bonding energies, thus having a net repulsive interaction balance with the environment. Obviously, the fraction of such molecules cannot increase significantly with decreasing pressure due to the thermodynamic stability constraints. Thus, an asymmetry of the distribution results at lower densities. At the lowest simulated pressure (dashed line in Figs. 3a-d) the distribution becomes bimodal, indicating that water molecules can be found in two energetically different environments with bonding energies distributed roughly around -20 kJ/mol and around 0 kJ/mol. While the latter part of the distribution is obviously due to non-bonded, free water molecules, the former one might be considered as an indication of the presence of significant amounts of hydrogen-bonded molecules even under these high-temperature, low-density conditions.

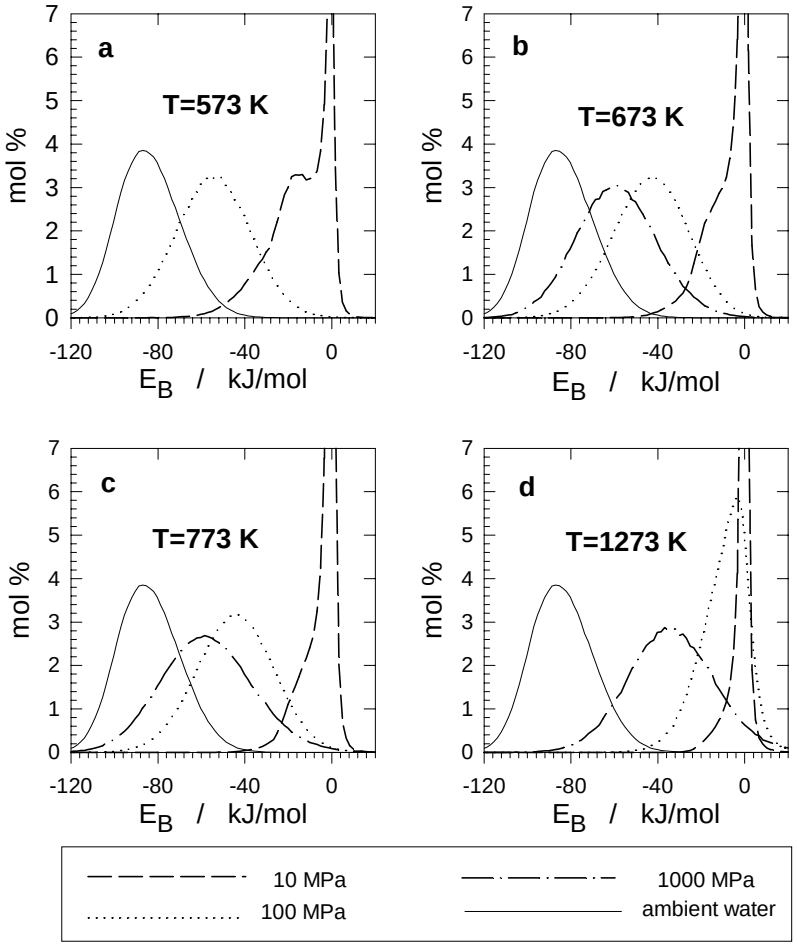

Figure 3. Normalized distributions of total intermolecular bonding energies for a water molecule in super-critical water. Units for the ordinate are mol % per kJ/mol.

The bonding energy distribution for the water molecules in liquid water at ambient conditions is also shown in Figure 3 as a thin solid line. At 773 K and 1000 MPa the density of supercritical water is virtually the same (≈1 g/cm^3) as that of liquid water at 298 K and 0.1 MPa. Therefore, the difference between the two distributions (thin solid and dash-dotted curves in Fig. 3c) can be considered as a pure effect of temperature. At the supercritical temperature the maximum is shifted by about 40 kJ/mol to higher (less negative) energies and the distribution becomes much wider. The comparison of both distributions clearly demonstrates that an individual water molecule experiences completely different energetic environments in these two thermodynamic states despite of the fact that densities (and, hence, average intermolecular distances) are virtually the same in both cases.

Pair energy distributions. Pair energy distributions represent another source of useful micro-thermodynamic information easily obtainable from computer simulations, but hardly measurable in real experiments. These functions, $p(E_{ij})$, represent the probability density of finding a pair of water molecules that have some particular interaction energy under given thermodynamic conditions. Figure 4 shows such functions for several typical thermodynamic states of supercritical water. Similar distribution for normal liquid water under ambient conditions is also shown in Figure 4 for comparison.

Independent of the thermo-dynamic conditions, most interactions in a bulk system

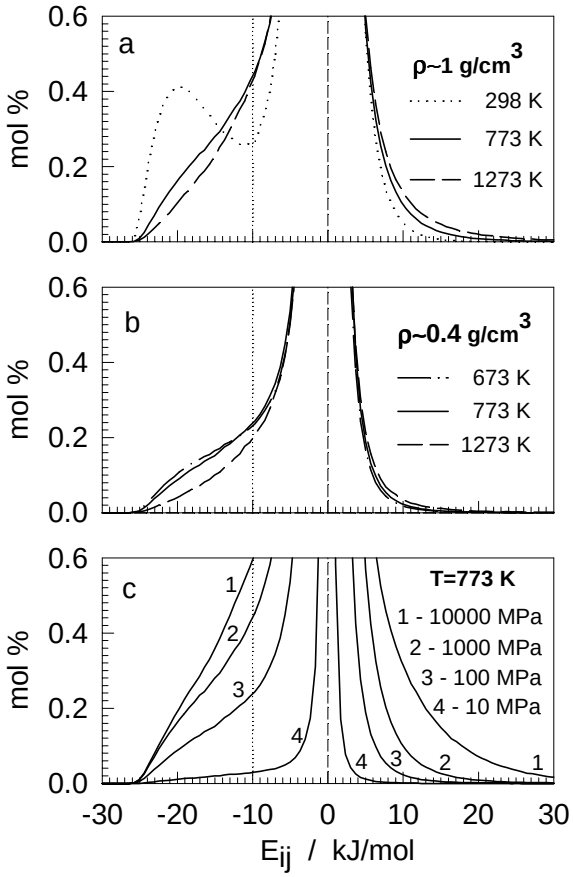

Figure 4. Normalized distributions of pair interaction energies (dimerization energies) in liquid and supercritical water. (a) At a constant density of 1 g/cm^3. (b) At a constant density of ≈0.4 g/cm^3. (c) At a constant temperature of 773 K.

involve pairs of rather distant molecules, resulting in the main peak of the distribution located around 0 kJ/mol. However, under ambient conditions (thick dotted line in Fig. 4a) there also exists a low-energy peak, which is commonly associated with the interactions of hydrogen-bonded neighbors. With decreasing density the main peak of the distribution becomes narrower with a higher maximum (beyond the scale in Fig. 4), because a relatively larger fraction of molecular pairs become separated by large inter-molecular distances with a near-zero interaction energy. The height of the low-energy peak decreases, but a distinct shoulder is clearly seen at the same range of energies, again qualitatively indicating the noticeable persistence of H-bonded molecular pairs even at the highest temperature and the lowest density studied.

The comparison of the distributions at 773 K and 1000 MPa and at 298 K and 0.1 MPa in Figure 4a presents once again the opportunity to see the pure effect of a significant temperature increase on the shape of the distribution along an isochore (densities at both thermodynamic states are ≈1 g/cm^3. The width and the height of the main maximum remain unchanged. However, in the attractive branch of the distribution (negative energies) a significant amount of molecular pairs are redistributed from the "hydrogen-bonding" range of energies (approximately between –25 and –15 kJ/mol) to the "non-bonding" range (approximately above –10 kJ/mol). In the repulsive (positive) branch, the probability for a molecular pair to have rather high interaction energy between +10 and +20 kJ/mol noticeably increases, confirming that repulsive interactions become a more important contribution to the thermodynamics of supercritical water.

Average potential energy. Average potential energy as a function of intermolecular distance, $\langle U_{ij}(r) \rangle$, is yet another source of helpful micro-thermodynamic information characterizing the energetic and geometric environment of an individual water molecule

under various thermodynamic conditions (Heinzinger and Vogel 1976; Kalinichev and Heinzinger 1992).

Such functions for the BJH and TIP4P water models at near-ambient (≈330 K) and supercritical (≈680 K) temperatures and a liquid-like density of 1 g/cm^3 are shown in Figure 5a along with the contributions arising from Coulomb and non-Coulomb parts of the corresponding intermolecular potentials. In contrast to the complex character of the non-Coulomb interaction in the BJH model, arising from the combination of OO, OH, and HH contributions (Eqns. 13–15), the only non-Coulomb contribution to the TIP4P model is the oxygen-oxygen Lennard-Jones term (Eqn. 12) and, hence, its contribution to $\langle U_{ij}(r)\rangle$ is both temperature- and density-independent (dotted line in Fig. 5b). Thus, in the case of the TIP4P potential only the change of the Coulomb part determines the differences between the average potential energies for different thermodynamic states, while in the case of the BJH potential the changes in Coulomb and non-Coulomb parts both contribute to the changes in $\langle U_{ij}(r)\rangle$ with temperature and/or density.

Figure 5 demonstrates that the BJH water model, in contrast to the TIP4P model, shows somewhat more preference for tetrahedrally ordered attractive molecular configurations (shallow minimum at OO distances ≈4.5 Å) even at supercritical temperature. However, the general features of the $\langle U_{ij}(r)\rangle$ functions are qualitatively and quantitatively very similar for both models, with the main minimum becoming less negative at a higher temperature.

Together with bonding energy distributions (Fig. 3), the average potential energy is a good tool for better understanding of the average energetic environment experienced by an individual water molecule under various thermodynamic conditions. The solid and the dashed lines in Figure 6a represent, respectively, the average potential energy for supercritical water at 773 K and 10 kbar, and for water under normal conditions with the TIP4P model employed in both cases. It is clear from the comparison, that the average energetic environment of a water molecule changes drastically as the temperature increases, despite of the fact that the average intermolecular distances remain unchanged

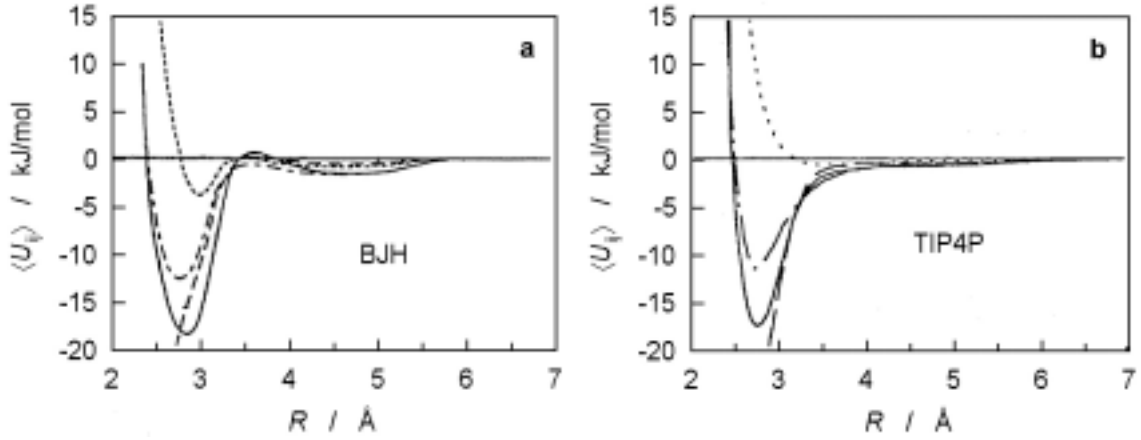

Figure 5. Average potential energy between two water molecules at liquid-like densities as a function of the oxygen-oxygen distance at two temperatures according to the BJH (a) and TIP4P (b) water models. a: Total (solid line), Coulombic (dashed line) and non-Coulombic (dotted line) components at T=336 K and ρ=0.97 g/cm^3 (Jancsó et al., 1984). Dash-dotted line is the total energy at T=680 K and the same density. b: Total (solid line), Coulombic (dashed line) and non-Coulombic (dotted line) components at T=323 K and ρ=1.03 g/cm^3. Dash-dotted line is the total energy at T=673 K and the same density.

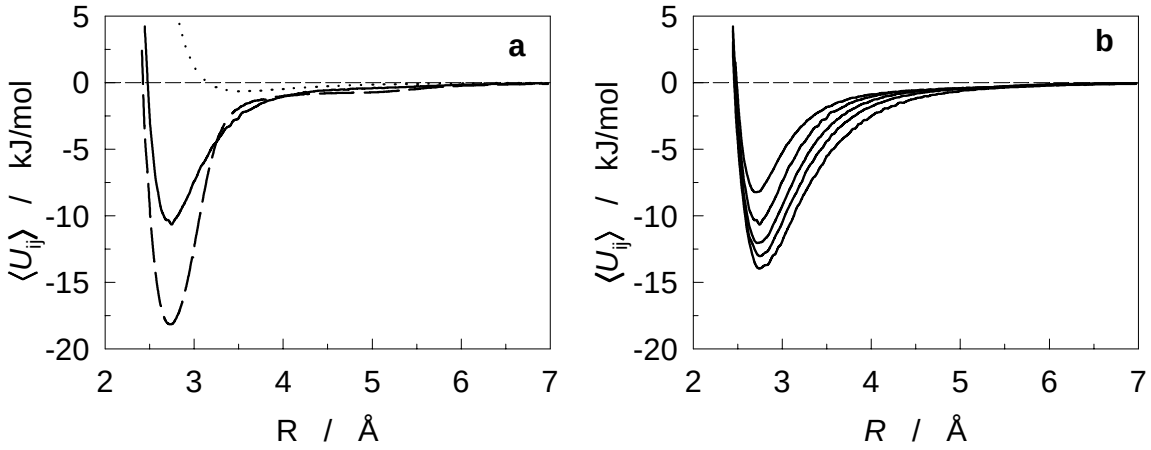

Figure 6. Distance dependence of the average potential energy between two water molecules in supercritical water. (a) Full line – 773 K and 1000 MPa; dashed line – 298 K and 0.1 MPa. The water density is virtually the same in both thermodynamic states. Dotted line – non-coulombic contribution to $\langle U_{ij}(r)\rangle$. (b) Pressure dependence along a supercritical isotherm of 773 K, from the bottom up: and 30, 100, 300, 1000, and 3000 MPa.

because of the nearly constant density. This is the consequence of a change in the average mutual molecular orientation due to the increased thermal motion (see the discussion of the structural properties in the next section). The shallow minimum around 4.5 Å in the Coulomb part of $\langle U_{ij}(r)\rangle$ which results from tetrahedral ordering of the molecules in liquid water completely disappears under supercritical conditions. The position of the potential minimum remains virtually unchanged while its depth decreases significantly with increasing temperature indicating that, on average, water molecules are bonded to each other almost half as strongly under supercritical conditions compared with ambient liquid water.

Figure 6b shows the effect of pressure (or density) increase on the average potential energy of between water molecules along a supercritical isotherm. It is clear from Figures 6a and 6b that both temperature and pressure act to decrease depth of the potential energy minimum – an indication of the weakening of hydrogen bonding (Kalinichev et al. 1999). The analysis of the water-water pair energy distributions and average water-water potential energies obtained from the simulations of aqueous electrolyte solutions under ambient conditions (Heinzinger and Vogel 1976; Heinzinger 1990) demonstrated that the effect of the dissolved ions on these functions is very similar to the effects of temperature and pressure. Thus, even more profound changes in these properties can be expected in the case of supercritical electrolyte solutions. The same conclusion can be drawn from structural properties of water and solutions, which are discussed in the next section.

STRUCTURE OF SUPERCRITICAL WATER

The most important information about the structure of a molecular liquid is calculated in molecular computer simulations in the form of atom-atom radial distribution functions, $g_{ij}(r)$. These functions give the probability of finding a pair of atoms i and j a distance r apart, relative to the probability expected for a completely random distribution of atoms at the same density.

The atom-atom radial distribution functions, $g_{OO}(r)$, $g_{OH}(r)$, and $g_{HH}(r)$ for two

supercritical states (773 K and 1273 K) at the density of normal liquid water, 1 g/cm^3, are shown in Figure 7 together with the results of simulations at 298 K and 0.1 MPa (dotted curves). The structure of water changes dramatically as the temperature rises to supercritical values, even at a liquid-like density. The characteristic second maximum of $g_{OO}(r)$ at 4.5 Å, reflecting the tetrahedral ordering of water molecules due to hydrogen bonding, is completely absent under these conditions, and a pronounced minimum of the distribution appears in its place. The comparison of the $g_{OO}(r)$ functions at ambient and supercritical temperatures shows a significant redistribution of nearest neighbors from the "hydrogen-bonding" regions of approximately 2.7-2.9 Å and 3.8-5.0 Å to the "non-bonding" region of 3.1-3.8 Å. It has been previously shown (Tanaka and Ohmine 1987) that precisely the pairs of molecules at intermediate distances are primarily responsible for repulsive interactions in liquid water, and these repulsions obviously increase under supercritical conditions. At the same time, the number of closest neighbors at distances up to ≈3.3 Å (the first minimum of $g_{OO}(r)$ in normal liquid water) remains unchanged.

The sharp first peak and following deep minimum of $g_{OH}(r)$ for normal liquid water (at 1.8 Å and 2.4 Å, respectively) become much less pronounced under supercritical conditions (Fig. 7b). These two characteristic features of $g_{OH}(r)$ observed in computer simulations, as well as experimentally (Soper et. al. 1997), are the basis of a simple geometric definition of a hydrogen bond, whereby the bond is assumed to exist between any pair of H_2O molecules whose respective O and H atoms are separated by less than R_{HB} = 2.4 Å. Integration under $g_{OH}(r)$ up to the chosen threshold distance provides a convenient way to quantitatively estimate the average number of H-bonds in which an individual molecule participates under various thermodynamic conditions (e.g., Kalinichev 1986; Mountain 1989; Guissani and Guillot 1993). At ambient conditions, this geometric criterion gives the average number of H-bonds per a water molecule $\langle n_{HB}\rangle_G$=3.2.

A detailed comparison of simulated structural functions for near-critical water with available neutron and X-ray diffraction data are shown in Figures 8 and 9. For the subcritical conditions of Figure 8, the agreement of the MC-simulated $g_{OO}(r)$, $g_{OH}(r)$, and $g_{HH}(r)$ functions for the TIP4P water model with the X-ray (Gorbaty and Demianets 1983) and neutron (Soper et al. 1997) diffraction data is very good. In fact, it is almost within experimental errors. The geometric estimates of the degree of hydrogen bonding give $\langle n_{HB}\rangle_G$=2.4 for both simulated and experimental $g_{OH}(r)$.

The disagreement of simulated and experimental radial distribution

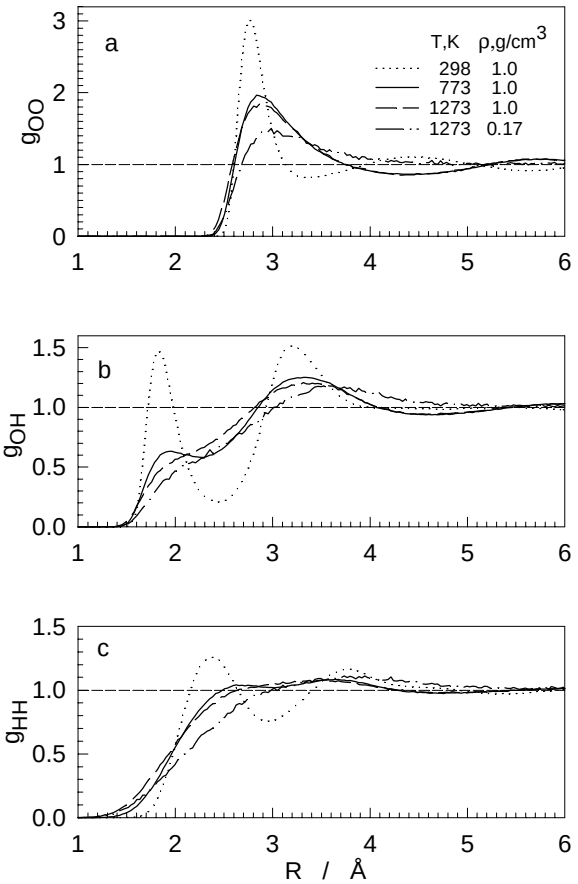

Figure 7. Atom-atom radial distribution functions for liquid and supercritical water at 1.0 g/cm^3 and 0.17 g/cm^3 from MC simulations with the TIP4P potential.

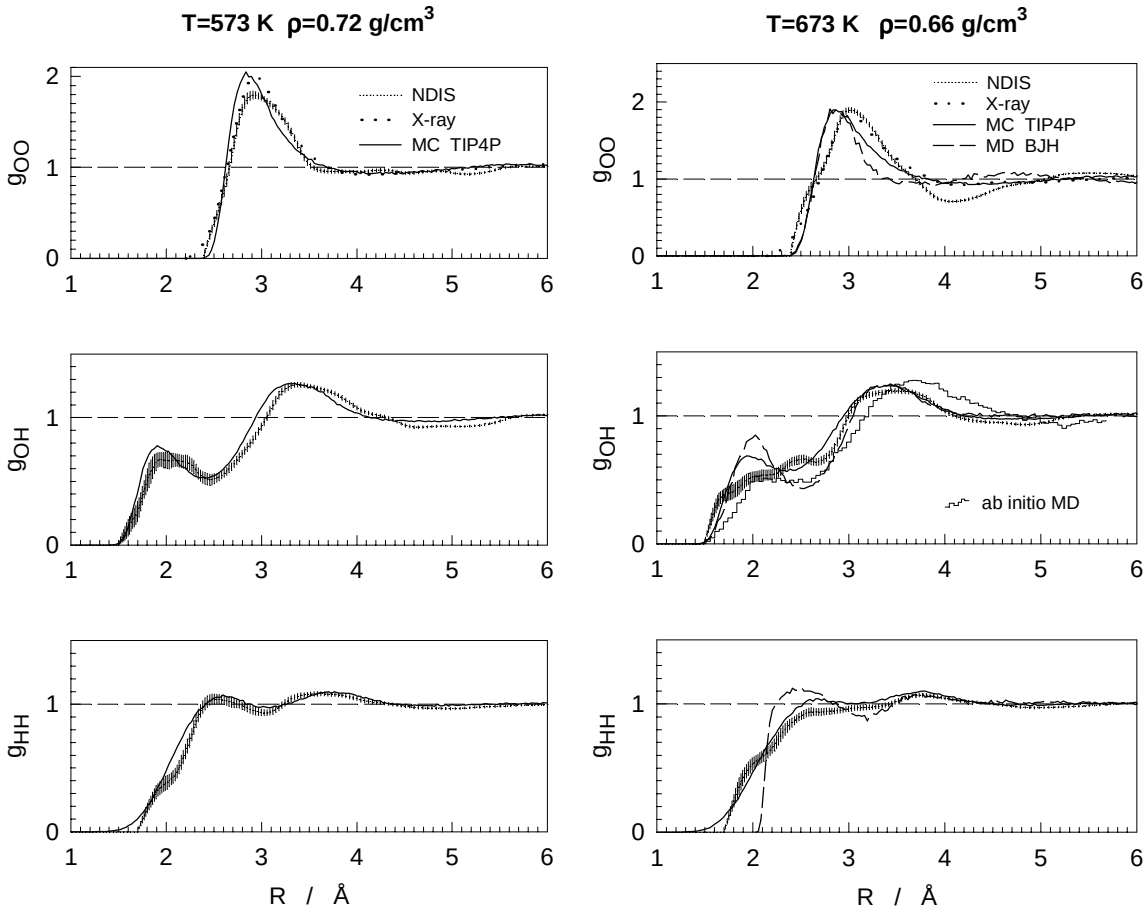

Figure 8 (left). Atom-atom radial distribution functions for subcritical water (T=573 K, ρ=0.72 g/cm^3) from MC simulations with the TIP4P potential (solid lines). Thick dotted line – X-ray diffraction (Gorbaty and Demianets 1983); thin dotted lines with error bars – neutron diffraction with isotope substitution, NDIS (Soper et al. 1997). [Reproduced with permission from *J Phys Chem A* 1997, *101*, 9720-9727. © 1997 American Chemical Society.]

Figure 9 (right). Atom-atom radial distribution functions for supercritical water (T=673 K, ρ=0.66 g/cm^3). Solid lines – MC simulations with the TIP4P potential; dashed lines – MD simulations with the BJH potential; thick dotted line – X-ray diffraction (Gorbaty and Demianets 1983); thin dotted lines with error bars – neutron diffraction (Soper et al., 1997); thin broken line – *ab initio* MD simulations (Fois et al. 1994). [Reproduced with permission from *J Phys Chem A* 1997, *101*, 9720-9727. © 1997 American Chemical Society]

functions is somewhat larger at the supercritical temperature of 673 K. In Figure 9 the results for the TIP4P model are presented together with two other computer simulations (Fois et al. 1994; Kalinichev and Heinzinger 1995) under very similar thermodynamic conditions. The structural functions simulated by Chialvo and Cummings (1994, 1996, 1999) for the SPC/E water model virtually coincide with results for the TIP4P model and are not shown in Figures 8 and 9. The simulations of Mountain (1995) for the ST2 and RPOL intermolecular potentials are also very close to the results for other water models.

The most striking feature of the neutron diffraction data at the supercritical temperature of 673 K (Fig. 9) is the disappearance of the first maximum of $g_{OH}(r)$ at ≈1.8 Å. However, a significant shoulder still remains at its place. This feature is best reproduced by the *ab initio* MD simulations of Fois et al.(1994) where no assumptions on

the interaction potential was *a priori* made. Molecular simulations for the TIP4P and SPC water models also come close to the neutron data, while the MD simulations with the flexible BJH water model show somewhat more structure in the $g_{OH}(r)$ function, compared to experimental data. The geometcic estimates of $\langle n_{HB} \rangle_G$ again give very close values of 2.1 for both experimental and TIP4P simulated distribution functions, while the BJH simulation gives the value of 2.3.

In all simulations, the $g_{OO}(r)$ and $g_{OH}(r)$ functions for several different water models are quite close to each other. However, the $g_{HH}(r)$ functions are significantly different in the case of the BJH potential, and demonstrate a much steeper rise of the distribution at ≈2 Å in disagreement with neutron diffraction data. In fact, the BJH potential is unable to correctly reproduce the behavior of this function because it explicitly forbids two hydrogens of different molecules to come closer than 2 Å to each other (Eqn. 15). This very strong H-H repulsion at the shortest intermolecular separations is also the main reason for the overestimation of pressure by the BJH potential (Kalinichev and Heinzinger 1992, 1995).

Although the general trends of the experimental radial distribution functions (such as the shift to larger distances and the broadening of the first $g_{OH}(r)$ peak with increasing temperature and decreasing density (Bruni et al. 1996; Soper et al. 1997) are qualitatively reproduced in the present simulations, these effects are less pronounced than observed in neutron diffraction measurements. Nonetheless, they are clearly seen in Figure 7 where the structural results of two extremely high-temperature (1273 K) MC simulations are shown for liquid-like and gas-like densities of supercritical water. With increasing temperature and decreasing density, the first peak of $g_{OH}(r)$ disappears due to the shifting and broadening, thus gradually filling the gap in the distribution between approximately 2 and 3 Å. With this specific hydrogen bonding peak becoming much less distinct at supercritical temperatures, the simple geometric criterion of H-bonding based exclusively on the analysis of $g_{OH}(r)$ distribution functions becomes very unreliable and additional orientational or energy constraints need to be taken into account (e.g., Kalinichev and Bass 1994; Chialvo and Cummings 1994; Soper et al. 1997).

HYDROGEN BONDING IN LIQUID AND SUPERCRITICAL WATER

In computer simulations, specific configurations of molecules, which can be considered as hydrogen-bonded, arise as a consequence of the charge distribution on individual water molecules. For a quantitative analysis of the H-bonding, various geometric constraints are often used in addition to the analysis of radial distribution functions. They are most frequently based on the requirement that one or several internal coordinates of a pair of water molecules (such as oxygen-oxygen distance, angles between some characteristic bond directions) fall within a certain specified range of values (Mezei and Beveridge 1981; Belch et al. 1981; Pálinkás et al. 1984; Chialvo and Cummings 1994; Mountain 1995; Soper et al. 1997).

However, in their early MD simulations of liquid water, Stillinger and Rahman (1972) have also introduced a simple energetic criterion of a hydrogen bond, which considers two molecules to be H-bonded if the interaction energy between them is lower than a given negative threshold. This criterion has been successfully applied to the analysis of temperature and density effects on the H-bond distributions in liquid and supercritical water (Jorgensen et al. 1983; Kalinichev and Bass 1994, 1995, 1997). Ideally, one should expect that the application of both—purely geometric or purely energetic—criteria should result in the same physical picture of hydrogen bonding. In practice however, both descriptions are not always consistent, especially under supercritical conditions.

The selection of the specific threshold energy value in the energetic criterion of hydrogen bonding is based on the analysis of pair energy distributions discussed earlier (Figs. 4a–c). The minimum of the distribution at about –10 kJ/mol is usually taken as the energetic cutoff threshold (E_{HB}) for hydrogen bonding under ambient conditions (Jorgensen et al. 1983). The integration under this low-energy peak up to E_{HB} gives another quantitative estimate of the number of H-bonds per a water molecule in the system, which is completely independent of any geometric considerations. It can be easily shown that for liquid water under ambient conditions this estimate virtually coincides with the simplest geometric estimate based on the analysis of the $g_{OH}(r)$ distribution function (Kalinichev and Bass 1994).

The variation of the energetic threshold value E_{HB} within reasonable limits does not qualitatively affect the picture of hydrogen bonding in liquid water which remains remarkably similar for a number of water-water interaction potentials used in computer simulations (Stillinger and Rahman 1972; Jorgensen et al. 1983; Rapaport 1983; Kalinichev and Heinzinger 1992; Kalinichev and Bass 1994; Mizan et al. 1996; Mahoney and Jorgensen 2000). Thus, adopting the same universal value of E_{HB}= –10 kJ/mol for all thermodynamic states provides a uniform and simple criterion for quantifying the picture of H-bonding at any temperature and density. It is also worth noting that this value of E_{HB} is quite consistent with spectroscopic and thermodynamic estimates of the hydrogen-bonding energy (Bondarenko and Gorbaty 1991; Walrafen and Chu 1995).

The picture of hydrogen bonding can be very efficiently visualized and analyzed by plotting intermolecular distance-energy distributions (Kalinichev and Bass 1994, 1997; Kalinichev et al. 1999), as shown in Figure 10. These distributions combine both $g_{OH}(r)$ and $p(E_{ij})$ functions into one 3-dimensional surface, where each point represents the relative probability of finding the hydrogen atom of a molecule i at a distance $R_{O...H}$ from

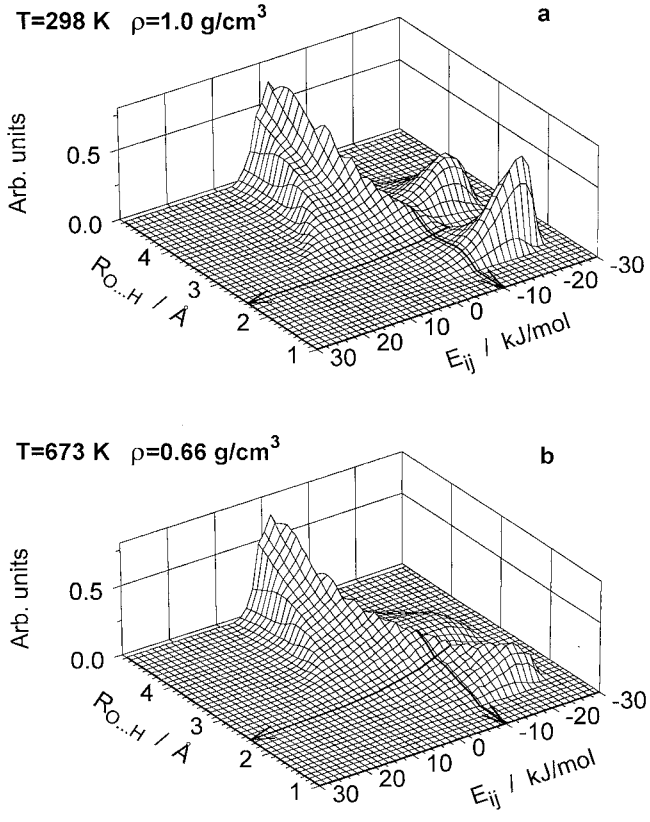

Figure 10. Normalized intermolecular O···H distance-energy distribution functions for liquid (a) and supercritical (b) water. Arrows show the cutoff values of the H-bond definition. [Reproduced with permission from *J Phys Chem A* 1997, *101*, 9720-9727. © 1997 American Chemical Society.]

the oxygen atom of a molecule j, with a specified interaction energy between the molecules of E_{ij}. From Figure 10a it is obvious that for liquid water under ambient conditions either geometric or energetic criteria both quite successfully and consistently distinguish H-bonded molecular pairs from the non-bonded ones, since the former are represented by the distinct low-energy short-distance peak on the distance-energy distribution surface around –20 kJ/mol and 1.8 Å. A weaker feature at the same energy range, but at distances around 3.3 Å obviously represents the most likely positions of the second hydrogen of the H-bonded molecule and corresponds to the second maximum of $g_{OH}(r)$ in Figures 7–9.

However, under supercritical conditions (Fig. 10b), the picture becomes much more complicated. The non-overlapping "tails" of the distance-energy distributions extend far beyond the chosen threshold values of HB energy and distance. Some of the molecular pairs considered as bonded in geometric terms often even have positive (repulsive) interaction energy, thus being obviously non-bonded in any reasonable physical sense. On the other hand, molecular pairs considered as H-bonded in energetic terms sometimes have an O···H separation as large as 3.0 Å, which also seems to be unreasonable.

The simplest geometric criterion of H-bonding based on the $g_{OH}(r)$ distribution function can, obviously, be made more selective by introducing additional spatial constrains on other interatomic separations and relative orientations of the interacting molecular pairs (Mezei and Beveridge,1981; Belch et al. 1981; Pálinkás et al. 1984; Chialvo and Cummings 1994; Mountain 1995; Soper et al. 1997). However, this inevitably jeopardizes the simplicity and universality of the criteria by increasing the number of more or less arbitrary chosen threshold parameters in the analysis. On the other hand, the simultaneous application of just two intermolecular cutoff criteria, one—distance-based (R_{HB}), and one—energy-based (E_{HB}) can be considered as the best compromise between simplicity and unambiguity of the constrains imposed on any molecular pair in order to distinguish between H-bonded and non-bonded configurations. Generally speaking, a chemical bond is most naturally described in terms of its length and strength, which is directly reflected in the hybrid distance-energy H-bonding criterion. Lifetime of a bond represents one more characteristic of H-bonding (e.g., Mountain 1995, Mizan et al. 1996), and will be briefly discussed in the next section.

Density and temperature dependencies of the average number of H-bonds, $\langle n_{HB} \rangle$, as well as those of average energy $\langle E_{ij} \rangle_{HB}$, distance $\langle R_{O\cdots H} \rangle_{HB}$, and angle $\langle \theta \rangle = \langle \angle O–H\cdots O \rangle$ of hydrogen bonds obtained from the present MC simulations by the application of thehybrid energetic and geometric criterion are presented in Figure 11. The average total energy of H-bonding is almost invariant over the entire density range at any given temperature. Although some smooth variation of the average HB angle $\langle \theta \rangle$ is clearly observable, it, too, remains almost constant over a very wide density range. Surprisingly enough, the angular HB distributions of the angle θ are also virtually density- (pressure-) independent along a supercritical isotherm (Fig. 12). Thus, at any particular temperature, the geometry of H-bonded molecular arrangements remains essentially the same over a very wide range of densities from dilute gas-like (~0.03 g/cm^3) to highly compressed liquid-like (~1.5 g/cm^3) fluid states. This fact, obviously, indicates that the growing orientational disorder, which accompanies the rise in temperature, is almost the sole mechanism of H-bond breaking under supercritical conditions.

Thus, we may conclude that the increase of temperature from ambient to supercritical affects the characteristics of H-bonding in water much more dramatically than the changes in density from 0.02 to 1.67 g/cm^3 along any supercritical isotherm. Compared to hydrogen bonds in ambient liquid water, H-bonds at 773 K are almost 2 kJ/mol weaker, have by 0.1 Å longer O··H bond distances, and are about 10° less linear.

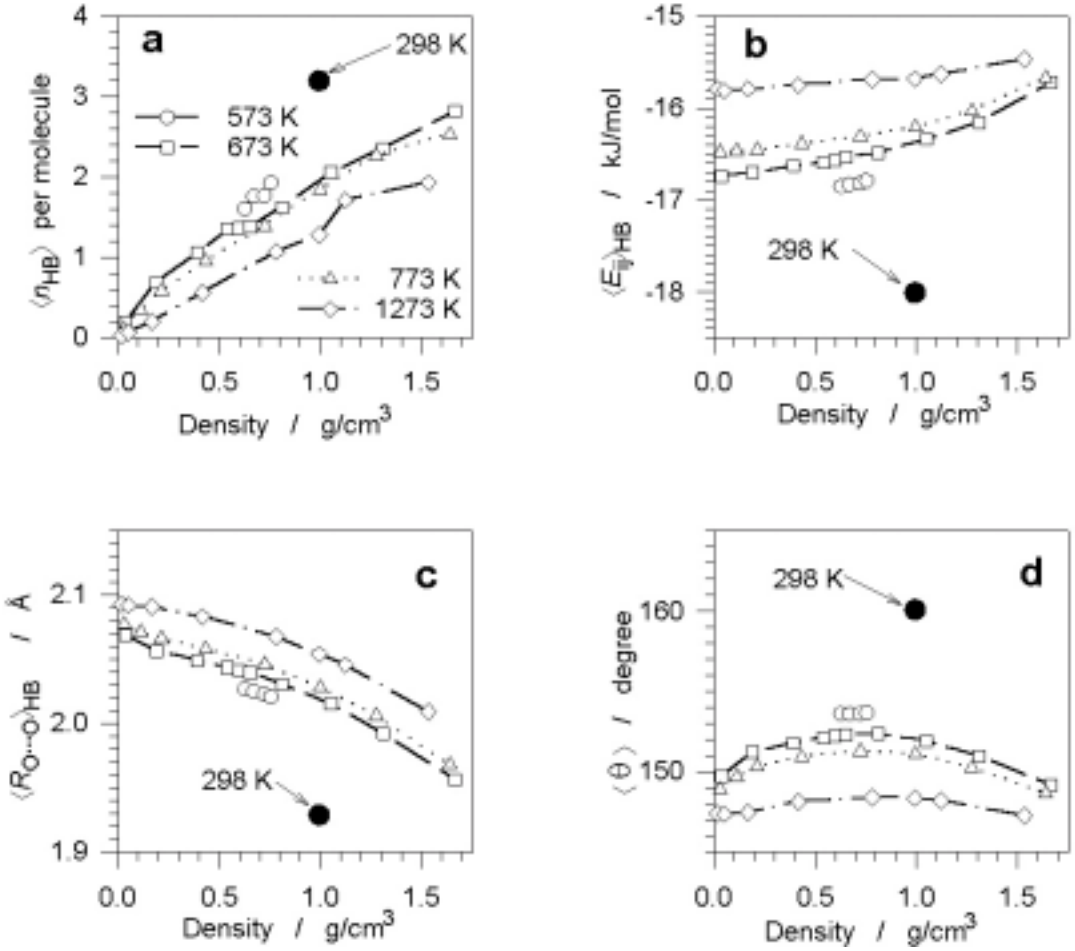

Figure 11. Average parameters of hydrogen bonds in liquid and supercritical water.

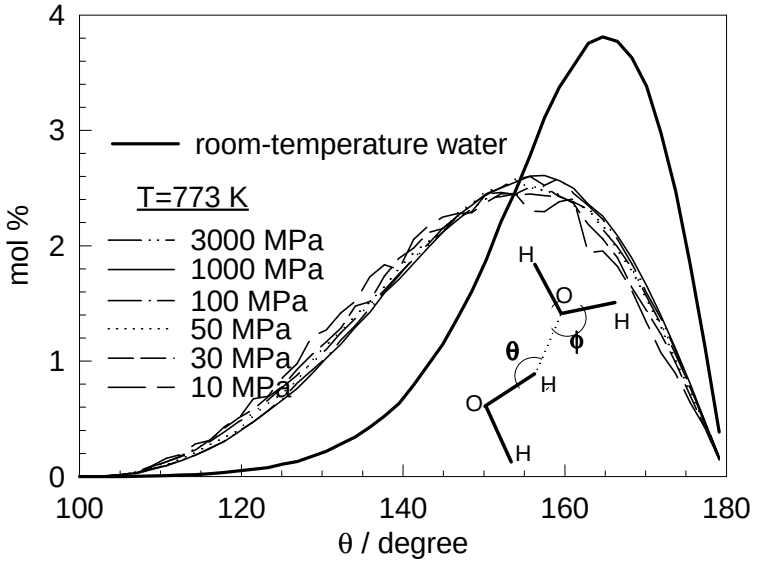

Figure 12. Distributions of H-bonding angles θ in liquid and supercritical water. Definitions of H-bonding angles θ and ϕ are given on the inset.

Figure 13 shows all available experimental estimates of $\langle n_{HB} \rangle$ from various sources (Gorbaty and Kalinichev 1995; Soper et al. 1997; Hoffmann and Conradi 1997; Matubayasi et al. 1997, 1999) overlapped with the results of Monte Carlo simulations for TIP4P water model under similar thermodynamic conditions. There is excellent agreement between experimental data and computer simulations (Kalinichev and Bass 1997; Chialvo and Cummings 1999). From computer simulations, the general temperature dependence of $\langle n_{HB} \rangle$ is observed as a broad band between high-density (dash-dotted) and low-density (dotted) curves, asymptotically approaching zero at higher temperatures and lower densities, as it was previously predicted (Gorbaty and Kalinichev 1995). Since these numbers of $\langle n_{HB} \rangle$ are well below the percolation threshold $n_p \approx 1.6$ (Blumberg et al. 1984), the percolating (i.e., continuous and infinite) tetrahedral network of hydrogen bonds is already broken at $T = 573$ K and $\rho < 0.63$ g/cm^3 (Fig. 13). For temperatures above 873 K, the continuous H-bonding network is broken even for liquid-like densities of $\rho \leq 1.0$ g/cm^3. However, even at the highest temperature and the lowest density there persist some noticeable degree of hydrogen bonding, represented, most probably, by small clusters like dimers and trimers.

Temperature and density dependencies of fractions of water molecules having a given number of H-bonds for a typical supercritical isobar and isotherm are plotted in Figure 14 based on the MC simulations for the TIP4P water model. For the thermodynamic conditions of neutron diffraction experiments (Soper et al. 1997), at 673 K and 0.66 g/cm^3, approximately 12% of water molecules are estimated to be involved in 3 H-bonds, about 70% of molecules involved in 1 or 2 H-bonds (dimers and trimers), and only 17% represent non-bonded monomers. This picture is in good qualitative agreement with semi-empirical calculations using equations of state for water based on the hydrogen bonding lattice fluid model (LFHB) (Gupta et al. 1992) and associated perturbed anisotropic chain theory (APACT) (Smits et al. 1994).

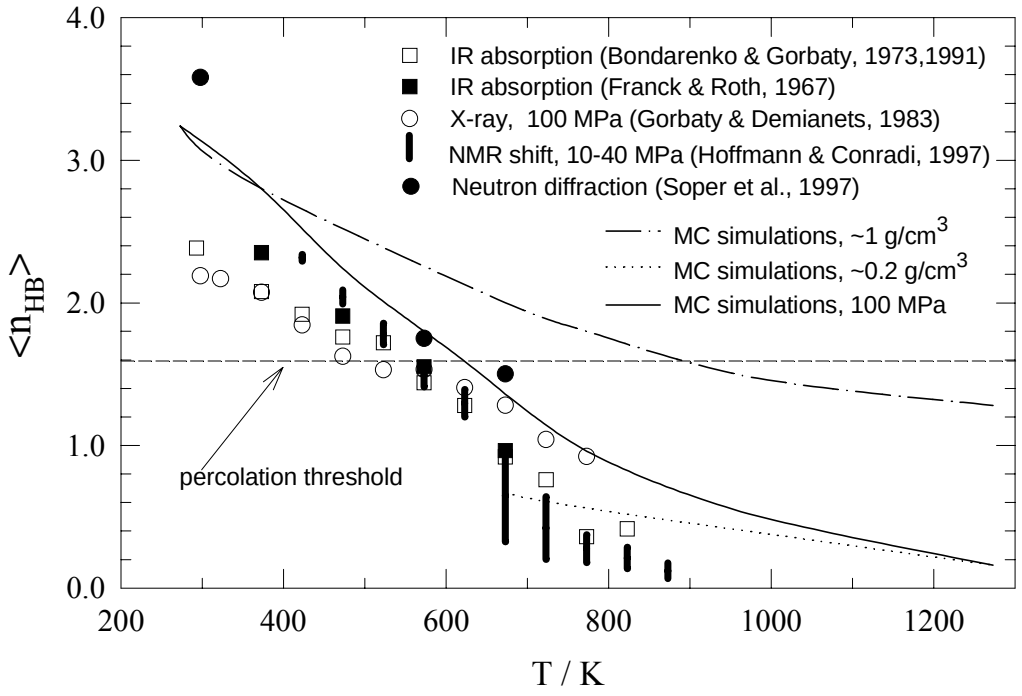

Figure 13. Temperature dependence of the average number of H-bonds per molecule, $\langle n_{HB} \rangle$, derived from computer simulations and experimental data. [Reproduced with permission from *J Phys Chem A* 1997, *101*, 9720-9727. © 1997 American Chemical Society.]

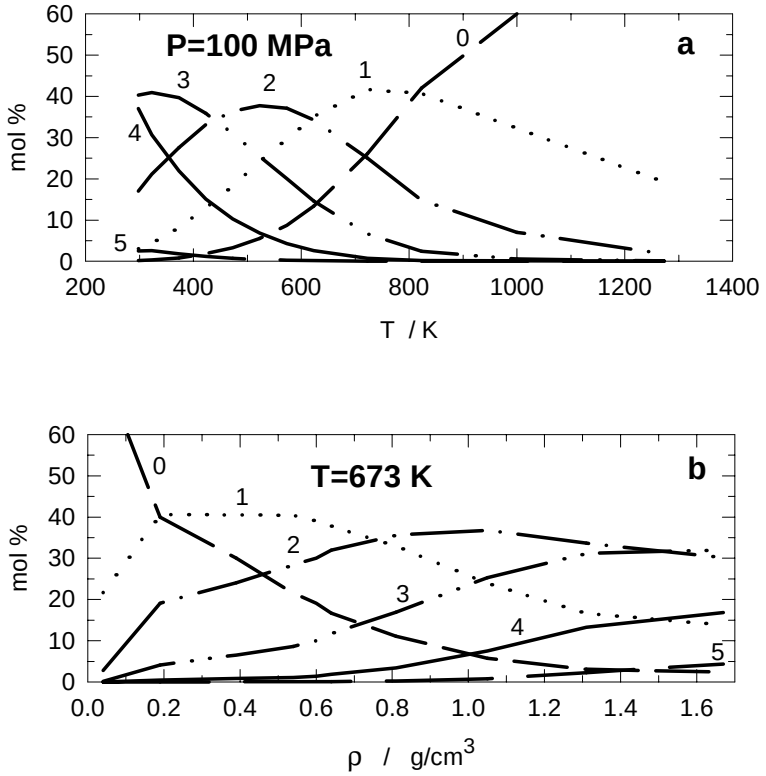

Figure 14. Distributions of water molecules involved in a given number of H-bonds (numbers at the curves) in supercritical water: (a) along an isobar of 100 MPa; (b) along an isotherm of 673 K.

MOLECULAR CLUSTERIZATION IN SUPERCRITICAL WATER

The formation of small molecular clusters in high temperature water vapor, as well as in supercritical fluid has recently attracted significant attention (Driesner 1997; Mountain 1999; Kalinichev and Churakov 1999, 2000). The nucleation of clusters results in local structural and density heterogeneity in the fluid. In different clusters water molecules possess slightly different properties such as the dipole moment and lengths of interatomic bonds (e.g., Ugdale 2000). So, topologically different water complexes may be even considered as distinct chemical species. Quantitative understanding of the size and structure of such clusters is important for many fundamental and practical reasons. For example, recent estimates suggest that the large effects of pressure on the isotope fractionation between high temperature aqueous solutions and minerals can be explained by the varying degree of clusterization in water vapor (Driesner 1997; Horita et al. 1999).

The application of the H-bonding criterion to every pair of molecules in a computer-generated configuration results in a connectivity matrix for this configuration. From it, the groups of molecules interconnected by a network of H-bonds can be easily identified to obtain cluster size distributions. By indexing the interconnected molecules, geometric and energetic characteristics of each isolated cluster can also be obtained. We consider here a molecule as belonging to a hydrogen-bonded cluster if it has at least one H-bond with some other molecule in the cluster. Following this definition, the maximum cluster size in computer simulations is limited by the total number of molecules in the simulation box. However, water molecules can be considered to form an infinite percolating H-bonded network, if a periodic image of at least one of them belonged to the same cluster as its origin.

It has been recently shown (Mountain 1999; Kalinichev and Churakov 1999) that the size of the H-bonded network under supercritical conditions is mainly controlled by water density. Simulations over a wide range of densities $0.03 < \rho < 1.5$ g/cm^3 allow us to trace gradual changes in the structure of supercritical water, from dilute vapor to dense liquid-like fluid. In Figure 15 cluster size distributions (normalized probabilities for a randomly selected molecule to participate in a cluster of a given size) are shown for several supercritical temperatures and densities ($T^* = T/T_c$, $\rho^* = \rho/\rho_c$), as well as for ambient liquid water. Dilute vapor consists mostly of individual monomers. However, even at ρ^*=0.12, up to 18 % of molecules form multi-molecular clusters. The largest water cluster observed under these conditions consisted of nine molecules, contributing 0.0026 % to the cluster size distribution. It is quite remarkable, that even at very low densities and high temperatures such large clusters may sometimes occur. As density increases, water molecules form even larger clusters. At a certain density, when the concentration of H-bonds reaches the percolation threshold, an infinite cluster of H-bonded molecules is formed. At a density above the percolation threshold molecules have

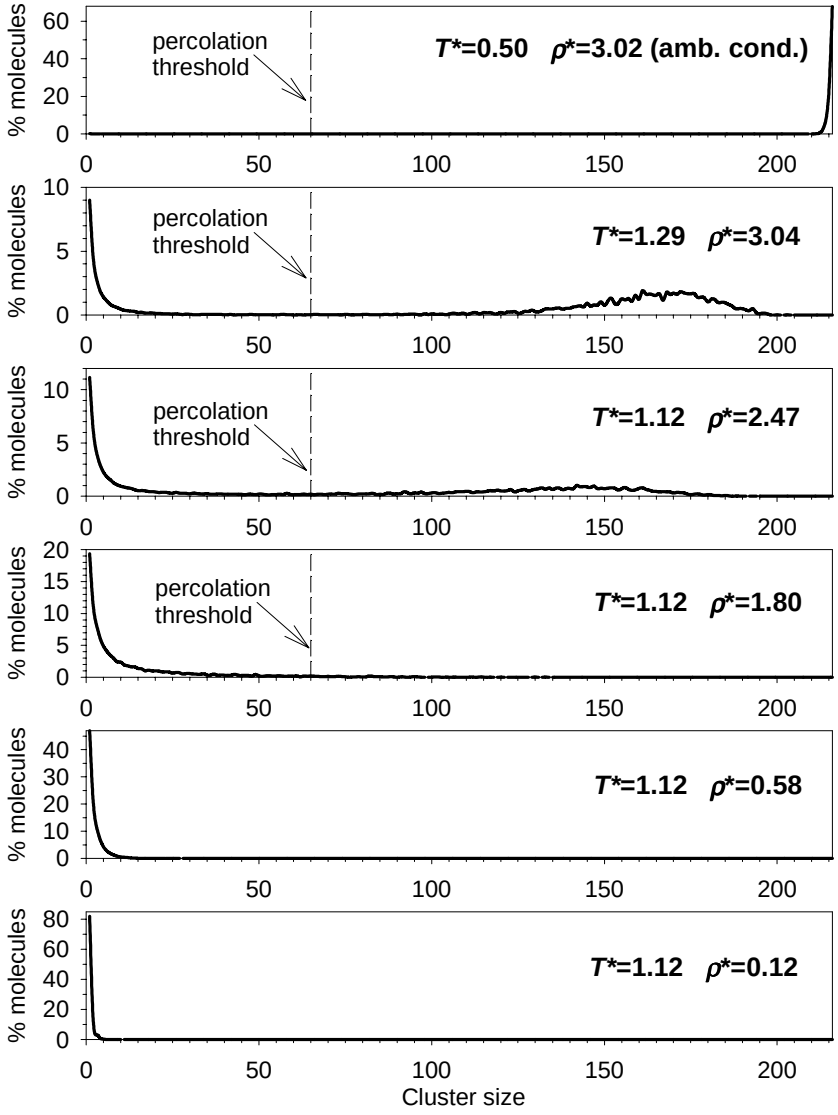

Figure 15. Participation of water molecules (%) in H-bonded clusters of different size under ambient and supercritical conditions.

a higher probability to join the percolating cluster. That decreases the fraction of molecules forming smaller isolated complexes, and, considering finite system size N, one can observe bimodal cluster size distributions.

We calculated the probability for the largest observed cluster to percolate depending on the hydrogen bond concentration, $\langle n_{HB} \rangle$, under various thermodynamic conditions (Churakov and Kalinichev 2000). From these data, the size of a percolating cluster at $T^* = 1.12$ is estimated to be ~65 molecules. This value divides cluster size distributions into two parts. One of them represents infinite percolating clusters, while another part represents smaller isolated clusters (Fig. 15).

The topology of water clusters observed under supercritical conditions can also be easily analyzed. In this analysis, we do not make any distinction between donor and acceptor types of hydrogen bonds originating at a particular water molecule. Thus, every molecule is depicted as a structureless dot in Figure 16, where all observable topological types of 3-, 4-, and 5-mers are shown along with their relative abundances (normalized as a fraction of molecules participating in clusters of certain type) under several supercritical thermodynamic conditions listed below in Tables 4 and 5.

Figure 16 demonstrates that, despite the obvious domination of the simplest linear chain-like clusters, more complex structures are also present. Since only instantaneous configurations were analyzed, some of the observed clusters might in reality have a rather short lifetime, and thus represent only transient structures. Nevertheless, all bonds in the observed clusters satisfied both geometric and energetic criteria for H-bonding, and none of the observed structures can be considered energetically unfavorable within the given definitions.

H-bonded molecular clusters containing open chain-like or tree-like structures are found to predominate over clusters containing cyclic ring-like elements. Average

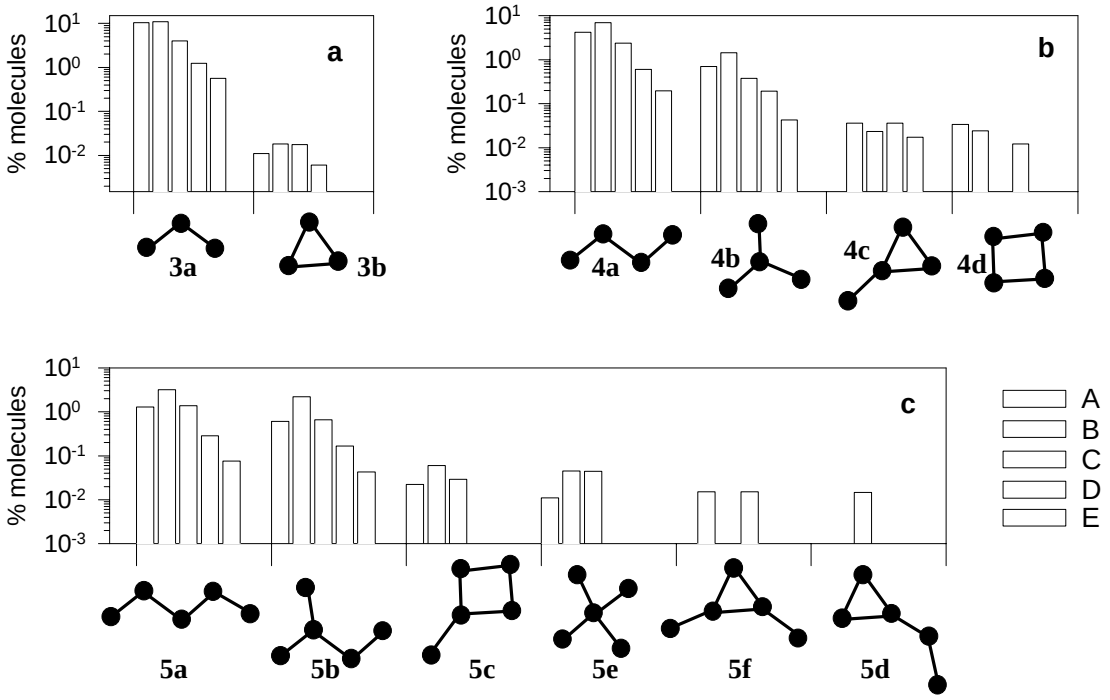

Figure 16. Topological types of H-bonded 3-mers, 4-mers, and 5-mers, and their relative abundance in supercritical BJH water. (See Table 4 for the thermodynamic conditions of runs A-E).

H-bonding angles, $\langle\angle O{\cdot\cdot}O{\cdot\cdot}O\rangle$ and $\langle\angle O{\cdot\cdot}H{-}O\rangle$, distances, $\langle R_{O\cdot\cdot O}\rangle$ and $\langle R_{O\cdot\cdot H}\rangle$, and energies $\langle U_{HB}\rangle$, of H-bonds forming the most abundant molecular 3-mers, 4-mers and 5-mers in supercritical water at $T^* = 1.04$ and $\rho^* = 1.13$ are reported in Table 2. It is remarkable, that the most abundant clusters, with topologies 3a, 4a, 4b, 5a, and 5b have almost identical geometric and energetic characteristics. So, H-bond lengths were found for all clusters to be ~2.04 Å, while H-bonding angles $\langle\angle O{\cdot\cdot}O{\cdot\cdot}O\rangle$ have values ~109°, which corresponds to the geometry of an ideal tetrahedrally ordered lattice. Cluster geometry was also studied at other thermodynamic conditions. With increasing temperature and/or decreasing density H-bond distances $\langle R_{O\cdot\cdot O}\rangle$ and $\langle R_{O\cdot\cdot H}\rangle$ increase, which is in agreement with previous observations (Kalinichev and Bass 1994, 1997; Mizan et al. 1994). However, average angles $\langle\angle O{\cdot\cdot}O{\cdot\cdot}O\rangle$ for the most abundant clusters remain almost constant at ~109° over the whole range of supercritical conditions studied. This result is in excellent agreement with earlier X-ray diffraction data for supercritical water (Gorbaty and Demianets 1983; Gorbaty and Kalinichev 1995) which show a noticeable peak of molecular distribution function at ~4.5 Å corresponding to tetrahedrally ordered second nearest neighbors.

There are two ways to compare cluster energies—energy per H-bond, or energy per molecule. These quantities are different, since clusters of the same size may have different number of internal bonds (Fig. 16). Because our cluster definition is based on the strength of its bonds, we use $\langle U_{HB}\rangle$ to characterize the energy of the clusters. Generally, one may expect the cluster abundance to be proportional to $\exp(-\beta U)$, where $\beta = (k_B T)^{-1}$, and U – potential energy of intermolecular interactions. At a given temperature, the most abundant clusters generally should have lower energy. This assumption, however, is not always supported by the data in Table 2. So, $\langle U_{HB}{}^{3a}\rangle < \langle U_{HB}{}^{3b}\rangle$, $\langle U_{HB}{}^{4a}\rangle < \langle U_{HB}{}^{4b}\rangle < \langle U_{HB}{}^{4c}\rangle$. On the other hand, $\langle U_{HB}{}^{4d}\rangle < \langle U_{HB}{}^{4a}\rangle$, in contrast with the low abundance of 4-member rings. Similarly, $\langle U_{HB}{}^{5e}\rangle \approx \langle U_{HB}{}^{5b}\rangle$, while the latter topology is much more abundant. We may conclude, that along with purely energetic considerations, entropic effects also play significant role in determining the abundance of particular cluster types. For instance, despite low potential energy of the configuration 5e, such pentamers can form only when very specific conditions for mutual distances and angles are simultaneously satisfied for all 5 molecules contributing to such a structure.

The dynamic nature of hydrogen bonding and the effects of temperature and density on the persistence of H-bonds in supercritical water were recently studied in MD simulations by Mountain (1995) using the ST2 and RPOL intermolecular potentials, and by Mizan et al. (1996) using the SPC potential and its flexible version. These authors use

Table 2. Average geometric and energetic parameters of small H-bonded clusters under supercritical conditions of T^*=1.04, ρ^*=1.13.

Cluster topology	*3a*	*3b*	*4a*	*4b*	*4c*	*4d*	*5a*	*5b*	*5c*	*5d*	*5e*
$\langle\angle O{\cdot\cdot}O{\cdot\cdot}O_1\rangle$ / °	109	60	110	107	114	87	110	108	112	107	105
$\langle\angle O{\cdot\cdot}O{\cdot\cdot}O_2\rangle$ / °					60				86	60	
$\langle\angle O{\cdot\cdot}O{\cdot\cdot}O_3\rangle$ / °										119	
$\langle R_{O\cdot\cdot H}\rangle$ / Å	2.04	2.07	2.04	2.04	2.06	2.03	2.04	2.04	2.05	2.06	2.05
$\langle R_{O\cdot\cdot O}\rangle$ / Å	2.90	2.89	2.91	2.91	2.90	2.90	2.91	2.91	2.91	2.90	2.92
$\langle\angle O{\cdot\cdot}H{-}O\rangle$ / °	149	143	150	150	146	150	150	150	149	146	150
$\langle U_{HB}\rangle$ / kJ/mol	-16.9	-16.4	-16.9	-16.7	-16.3	-17.0	-16.9	-16.8	-16.7	-16.3	-16.8

two different approaches to the estimation of the hydrogen bonding lifetime, but both of them are based on the analysis of survival (with a certain temporal resolution $\Delta\tau$) of H-bonds in a series of MD-generated molecular configurations. While the choice of the geometric and energetic parameters in any hydrogen bond definition is more or less determined by the shape of the energetic surface for water dimer, the choice of the time resolution interval $\Delta\tau$ is much less obvious. It is clear, that at $\Delta\tau \to 0$ the resulting picture of H-bonding should be very close to the instantaneous one. On the other hand, $\Delta\tau$ must be sufficiently small compared to the average H-bond lifetime (Rapaport 1983). The latter, is, actually, the principal goal of the analysis, thus it cannot be known in advance. In a simplified approach, we can consider a hydrogen bond to exist continuously if it satisfies our chosen H-bonding criterion at the end of each consecutive time interval $\Delta\tau$ along the MD trajectory. Otherwise, the bond considered broken during this interval. An example of how temporal resolution $\Delta\tau$ can affect the statistics of hydrogen bonding under typical supercritical thermodynamic conditions for BJH water is presented in Table 3. It is clear that the time-averaged picture of H-bonding resulting from spectroscopic and diffraction measurements, as well as MC simulations, can only be considered an upper boundary estimate. Depending on the stringency of the lifetime H-bonding criterion used, the average number of H-bonds in the system can change by a factor of two, and even more. The average lifetime of H-bonds in supercritical water is estimated to be about 0.2-0.5 ps (e.g., Mountain 1995; Mizan et al. 1996), which is about an order of magnitude lower then typical lifetimes of hydrogen bonds in liquid water under ambient conditions (Rapaport 1983; Bopp 1987).

DYNAMICS OF MOLECULAR TRANSLATIONS, LIBRATIONS, AND VIBRATIONS IN SUPERCRITICAL WATER

In MD simulations, the dynamical behavior of a molecular fluid can be monitored in terms of velocity autocorrelation functions (VACF), which are calculated as

$$\langle \mathbf{v}(0) \cdot \mathbf{v}(t) \rangle = \frac{1}{N_\tau N} \sum_{i=1}^{N_\tau} \sum_{j=1}^{N} \mathbf{v}_j(t_i) \cdot \mathbf{v}_j(t_i + t) \tag{20}$$

where N denotes the number of particles, N_τ – the number of time averages, and $\mathbf{v}_j(t)$ – the velocity of particle j at time t.

Molecular center-of-mass velocity autocorrelation functions for several supercritical states of water are shown in Figure 17. Obviously, the VACFs decay faster at the higher density. The density dependence of these functions is very similar to that for water at normal temperatures (Jancsó et al. 1984), in agreement with the similarity in the pressure-induced changes of the structural properties discussed above.

Table 3. Average number of H-bonds per water molecule and concentration of H-bonded species in supercritical BJH water at 630 K and 0.692 g/cm^3 as a function of a lifetime criterion for H-bonds.

$\Delta\tau$ / *ps*	$\langle n_{HB} \rangle$	*% of monomers (0 bonds)*	*% of dimers (1 bond)*	*% of trimers (2 bonds)*	*% of tetramers (4 bonds)*
0.01	1.41	16.6	39.4	31.9	10.7
0.1	0.83	40.2	40.2	16.3	3.0
0.2	0.57	55.0	34.2	9.5	1.2

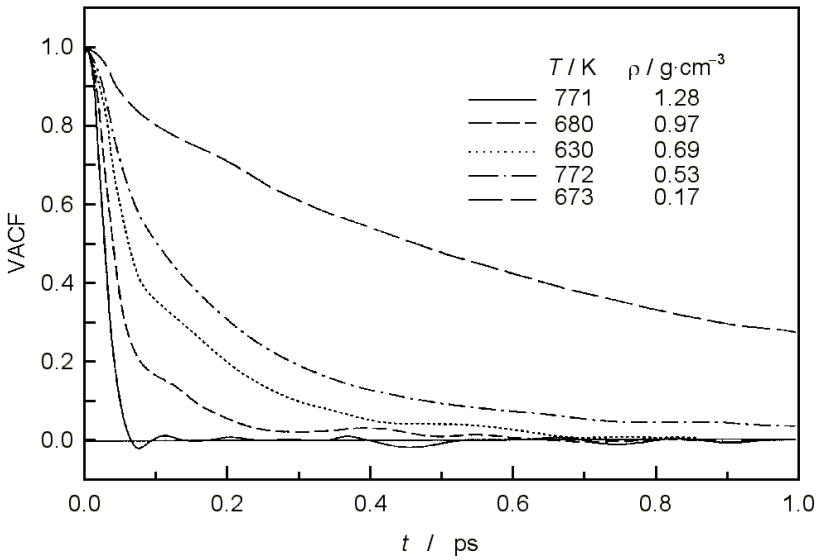

Figure 17. Normalized center of mass velocity autocorrelation functions for the water molecules under supercritical conditions.

Self-diffusion coefficients in supercritical water can be determined from MD simulations through the molecular mean-square displacement analysis, or through the velocity autocorrelation functions (Eqn. 20) with the help of the Green-Kubo relation (Allen and Tildesley 1987):

$$D = \lim_{t\to\infty} \frac{1}{3} \int_0^t \left\langle \mathbf{v}(0) \cdot \mathbf{v}(t') \right\rangle \, \mathrm{d}t' \tag{21}$$

The self-diffusion coefficients calculated for several supercritical thermodynamic states of BJH water are compared with available experimental data and the results of other computer simulations in Table 4**.** The statistical uncertainty of the calculated values is about 10%, i.e., comparable with the accuracy of experimental data. Thus, the simulated values of *D* agree very well with experiments. It is also quite surprising that

Table 4. MD-simulated self-diffusion coefficients of supercritical water.

MD-Run	*A*	*B*	*C*	*D*	*E*
ρ / g cm^{-3}	0.1666	0.5282	0.6934	0.9718	1.2840
T / K	673	772	630	680	771
D / 10^{-5} cm^2 s^{-1}	196	76	37	23	11
	193[(a)]	68[(a)]	44[(a)]	–	–
	>170[(b)]	68[(b)]	45[(b)]	22[(b)]	15[(b)]
		65[(c)]		24[(d)]	
				23[(e)]	

[(a)] NMR spin-echo measurements of Lamb et al. (1981).
[(b)] MD simulations for the TIP4P water model (Brodholt and Wood 1990, 1993a).
[(c)] MD simulations for the SPC water model. Interpolated from (Mizan et al. 1994).
[(d)] MD results for the BNS rigid water model at 641 K (Stillinger and Rahman 1972).
[(e)] MD results for the Carravetta-Clementi potential (Kataoka 1989).

three other high-temperature MD simulations (Stillinger and Rahman 1972; Kataoka 1989; Brodholt and Wood 1990, 1993) at a density of ≈1 g/cm^3, with three different intermolecular potentials, resulted in self-diffusion coefficients virtually identical to that of the run D for the BJH model. This seems to indicate that all the intermolecular potentials are able to reproduce correctly the temperature dependence of the self-diffusion coefficients up to supercritical temperatures at least at liquid-like densities. It also indicates that calculations of self-diffusion coefficients from MD simulations are not very sensitive to the details of the particular intermolecular potential used.

The pronounced effects of temperature and density are also reflected in the spectral densities of the hindered translational motions of water molecules, which can be calculated by Fourier transformation of the velocity autocorrelation functions (e.g., Allen and Tildesley 1987). Such spectra for two high-density supercritical MD simulations (Kalinichev and Heinzinger 1992; Kalinichev 1993) are shown in Figure 18 as dotted and dash-dotted lines, while similar spectra for near-ambient liquid water are shown as solid and dashed lines for the BJH and SPC models, respectively. In normal liquid water, the peaks at ~60 cm^{-1} and ~190 cm^{-1} are usually assigned to the hydrogen bond O··O··O bending motion and O··O stretching motions, respectively (e.g., Eisenberg and Kautzmann 1969). Both peaks completely disappear at supercritical temperature, indicating a significant break down of the H-bonding water structure. It is also important to note that the decrease of the spectral intensities in the low-frequency range of the H-bond bending and stretching motions is quite similar to the effect of dissolved ions (e.g., Szász and Heinzinger 1983a,b).

For a flexible water model, one can calculate the changes in the average geometry of the molecules brought about by the changes of the thermodynamic conditions. The simulated average intramolecular geometric parameters of molecules in supercritical BJH water are given in Table 5. The corresponding values for an isolated BJH water molecule and for the molecules in ambient liquid water are 0.9572 and 0.9755 Å for the intramolecular OH distance, 104.52° and 100.78° for the intramolecular HOH angle, and 1.86 and 1.97 Debye for the dipole moment, respectively (Jancsó et al. 1984). Comparing these values with the data in Table 5, one can see that the increase of density, and that of temperature (at the normal liquid-like density of the run D), both lead to an elongation of the average intramolecular OH distance and a decrease of the average HOH angle. Due to

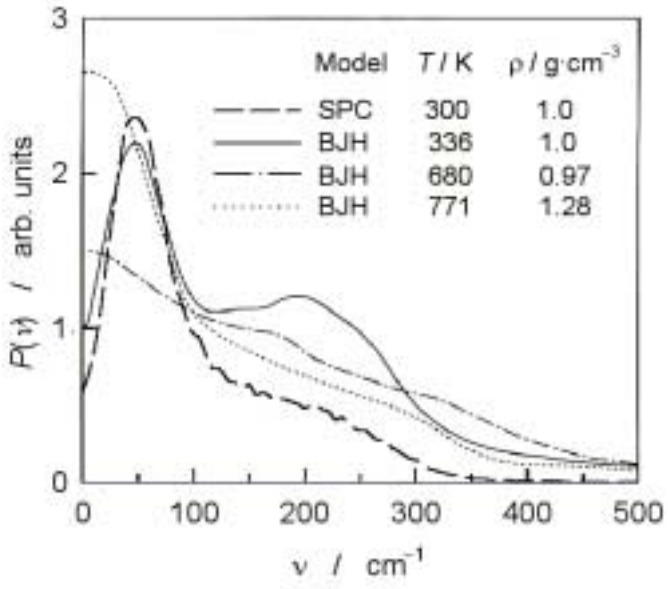

Figure 18. Spectral densities (in arbitrary units) of low-frequency translational motions for super-critical water at liquid-like densities. The spectra of liquid water under ambient conditions for the BJH (Jancsó et al. 1984) and SPC water models are given for comparison.

Table 5. Intramolecular geometry and vibrational frequencies of supercritical BJH water.

MD-Run	*A*	*B*	*C*	*D*	*E*
ρ / g cm^{-3}	0.1666	0.5282	0.6934	0.9718	1.2840
T / K	673	772	630	680	771
$\langle R_{OH} \rangle$ / Å	0.9705	0.9750	0.9755	0.9781	0.9811
$\langle \angle HOH \rangle$ / °	102.00	100.82	100.28	99.51	98.26
$\langle \mu \rangle$ / Debye	1.99	2.02	2.03	2.05	2.07
ν_1^{max} / cm^{-1}	3640	3580	3500	3530	3415
	3625[(a)]	3585[(a)]	3567[(a)]	–	–
	3630[(b)]	3595[(b)]	3567[(b)]	3550[(b)]	–
	3600[(c)]	3580[(c)]	3569[(c)]	–	3527[(d)]
FWHM$_1$ / cm^{-1}	230	300	340	360	470
ν_2^{max} / cm^{-1}	1660	1670	1690	1700	1730
FWHM$_2$ / cm^{-1}	110	130	130	190	400
ν_3^{max} / cm^{-1}	3760	3690	3675	3630	3570
FWHM$_3$ / cm^{-1}	180	280	290	310	450

[(a)] Raman spectroscopic data of Frantz et al. (1993).
[(b)] Raman spectroscopic data of Lindner (1970).
[(c)] IR spectroscopic data of Gorbaty (1979).
[(d)] Raman spectroscopic data of Walrafen et al. (1988) at 443 K and 3300 MPa.

the presence of partial charges on O and H atoms, these both factors increase the average dipole moment of the water molecules with increasing temperature and density. The same temperature dependence of the average intramolecular geometry can be deduced from the comparison of the run E in Table 5 and the high-density simulation of Jancsó et al., (1984) at 350 K and 1.346 g/cm^3, which resulted in $\langle R_{OH} \rangle = 0.9767$ Å, $\langle \angle HOH \rangle = 99.82°$, and $\langle \mu \rangle = 1.992$ Debye.

The rotational relaxation of water molecules is often discussed in terms of angular momentum autocorrelation functions (e.g., Stillinger and Rahman 1972; Yoshii et al. 1998). For a flexible water model, a slightly different approach can also be used. In order to separate the various modes of molecular librations (hindered rotations) and intramolecular vibrations, the scheme proposed by Bopp (1986) and Spohr et al. (1988) can be employed. The instantaneous velocities of the two hydrogen atoms of every water molecule in the molecular center-of-mass system are projected onto the instantaneous unit vectors: i) in the direction of the corresponding OH bond ($\mathbf{u_1}$ and $\mathbf{u_2}$); ii) perpendicular to the OH bonds in the plane of the molecule ($\mathbf{w_1}$ and $\mathbf{w_2}$); and iii) perpendicular to the plane of the molecule ($\mathbf{v_1}$, and $\mathbf{v_2}$). Then the following six quantities can be defined using capital letters to denote the projections of the hydrogen velocities onto the corresponding unit vectors:

$$R_X = W_1 - W_2 \tag{22}$$

$$R_Y = V_1 + V_2 \tag{23}$$

$$R_Z = V_1 - V_2 \tag{24}$$

$$Q_1 = U_1 + U_2 \tag{25}$$

$$Q_2 = W_1 + W_2 \tag{26}$$

$$Q_3 = U_1 - U_2 \tag{27}$$

The quantities R_X, R_Y, and R_Z approximate instantaneous rotational motions around the three orthogonal principal axes of the water molecule, and Q_1, Q_2, and Q_3 approximately describe the three normal modes of molecular vibrations usually referred to as symmetric stretch, bend, and asymmetric stretch, respectively (schematically illustrated on the inserts in Fig. 19).

The dynamics of different modes of molecular librations (hindered rotations) and intramolecular vibrations in supercritical water can now be analyzed in terms of velocity autocorrelation functions for the corresponding projections (Eqns. 22–27) (Kalinichev and Heinzinger 1992, 1995; Kalinichev 1993). The velocity autocorrelation functions calculated for the quantities Q_i (Eqns. 25–27) are shown in Figure 19 for two extreme cases of high-density and low-density supercritical water. The Fourier transforms of these functions result in the spectral densities of the corresponding vibrational modes. They are shown in Figure 20 for the supercritical thermodynamic states listed in Table 5.

The frequencies of the vibrational peak maxima and the widths at half maximum, FWHM, are also given in Table 5. The error bounds for the calculated frequencies are estimated to be about $\pm 30 cm^{-1}$ (Kalinichev and Heinzinger 1992, 1995). There is an empirical relationship (La Placa et al. 1973) for the rate of decrease of the OH stretching frequency in response to the decreasing intramolecular OH distance ($\approx$20,000 cm^{-1}/Å), which seems to hold well for simulations of aqueous electrolyte solutions at room temperature and liquid-like densities (Heinzinger 1990). From this relationship and changes of the average intramolecular geometry discussed above, a *red shift* of about 55 cm^{-1} relative to liquid water at normal temperature is expected for the vibrational

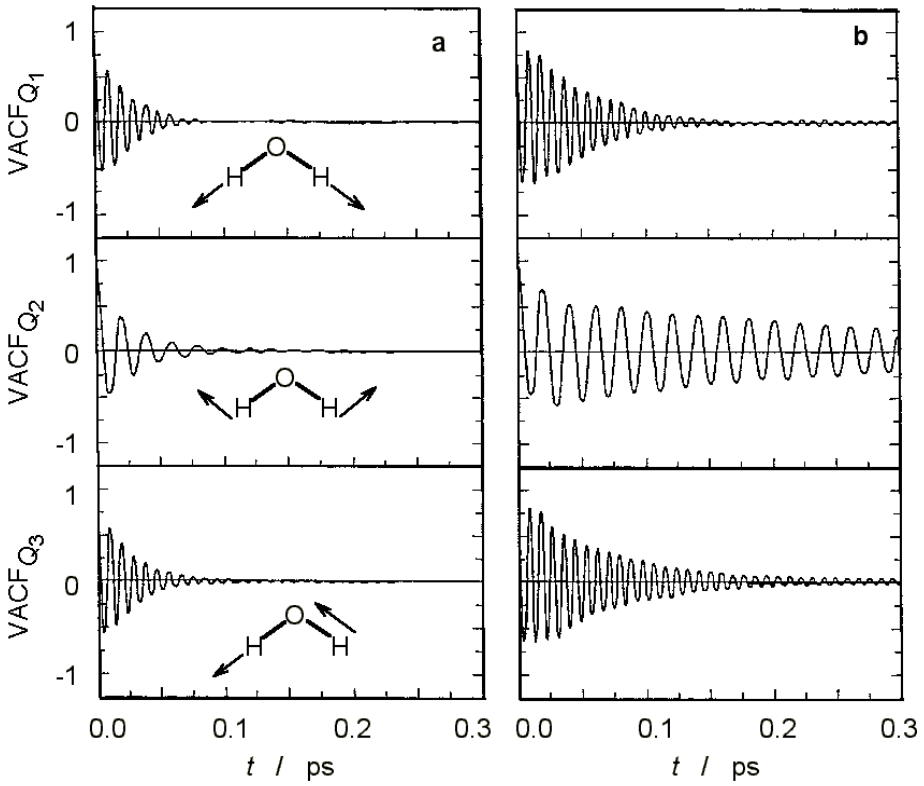

Figure 19. Velocity auto-correlation functions for the three intramolecular vibrations of water molecules at supercritical temperatures: (a) 771 K, 1.284 g/cm^3; (b) 673 K, 0.166 g/cm^3. Q_1, Q_2, and Q_3 denote the symmetric stretching, bending, and asymmetric stretching modes, as illustrated on the inserts.

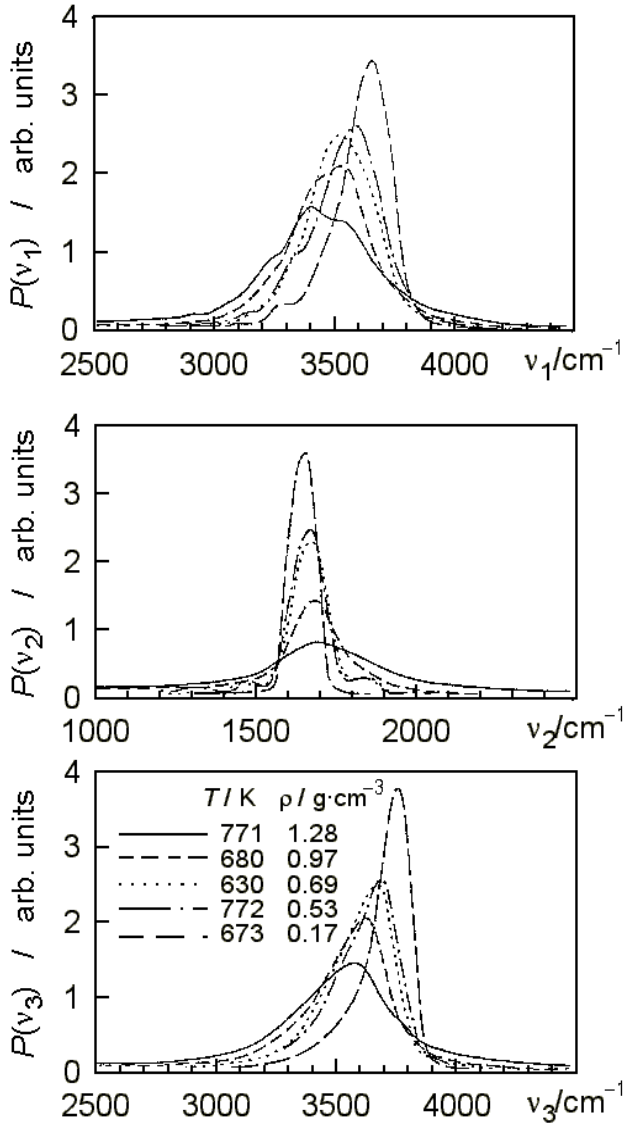

Figure 20. Spectral densities (in arbitrary units) of the intramolecular vibrations of supercritical water from MD simulations. ν_1, ν_2, and ν_3 denote the symmetric stretching, bending, and asymmetric stretching modes, respectively.

frequencies of the run D (at a supercritical temperature of 680 K, but at a density close to that of normal liquid water, ≈1 g/cm^3). However, based on the symmetric stretching frequency for liquid BJH water under ambient conditions, ν_1=3475 cm^{-1} (Bopp 1986), a *blue shift* of approximately the same magnitude is estimated in reasonable agreement with Raman spectroscopic data (Lindner 1970; Kohl et al. 1991) where a blue shift of about 120 cm^{-1} was observed. Clearly, the simple empirical relationship is not applicable any more when both temperature and density (pressure) can simultaneously affect the average intramolecular geometry.

Raman and infrared spectroscopic data for supercritical water (Lindner 1970; Gorbaty 1979; Frantz et al. 1993), interpolated where necessary, are given in Table 5 for comparison with MD simulations. It is a common practice in high-pressure spectroscopic experiments to describe results in terms of spectral shifts per unit of pressure, cm^{-1}/MPa

(Walrafen 1973; Klug and Whalley 1984; Farber et al. 1990). However, density would be a much more appropriate variable, as the one more directly related to the changes of interatomic distances taking place with increasing pressure. Frantz et al. (1993) have shown that while Raman spectra of water demonstrate significant pressure dependence along an isotherm, as well as temperature dependence along an isobar, they are virtually independent of temperature at any particular density over a very wide range from vapor-like to liquid-like densities at temperatures above 520 K.

The density dependence of the frequency of spectral maxima ν_1^{max} obtained in the MD simulations of BJH water is compared in Figure 21 with all available experimental data. One point from high-pressure, high-temperature Raman measurements of Walrafen et al. (1988) is also plotted in Figure 21 for comparison, although it corresponds to a somewhat lower temperature and higher pressure (443 K and 3300 MPa, respectively) than those used in the simulations. Except for one point, there is a remarkable agreement between simulated and measured values.

The large discrepancy for the run C at 0.6934 g/cm^3 (see Table 5) could possibly be related to the fact that it was the only MD-simulation in this series actually performed at subcritical temperature, 630 K, and thus could correspond to a metastable thermodynamic state. An indirect indication of this might also be seen in the discrepancy of pressure calculated for the same point (Kalinichev and Heinzinger 1992; 1995), which was also far beyond the qualitatively reasonable representation of the equation of state observable for all other simulation points. However, more extensive simulations for the BJH water over wider ranges of temperature and density need to be performed before the phase diagram for this particular water model could be better understood.

The bending frequency ν_2 of liquid BJH water under ambient conditions is 1705±5 cm^{-1} (Bopp et al. 1983; Heinzinger 1990) compared to 1644^{-1} in real liquid water (Falk 1990). This frequency does not change much with temperature in MD simulations (cf. run D in Table 5) in perfect agreement with Raman measurements of Ratcliffe and Irish (1982) who found that bending frequency shows no temperature dependence within

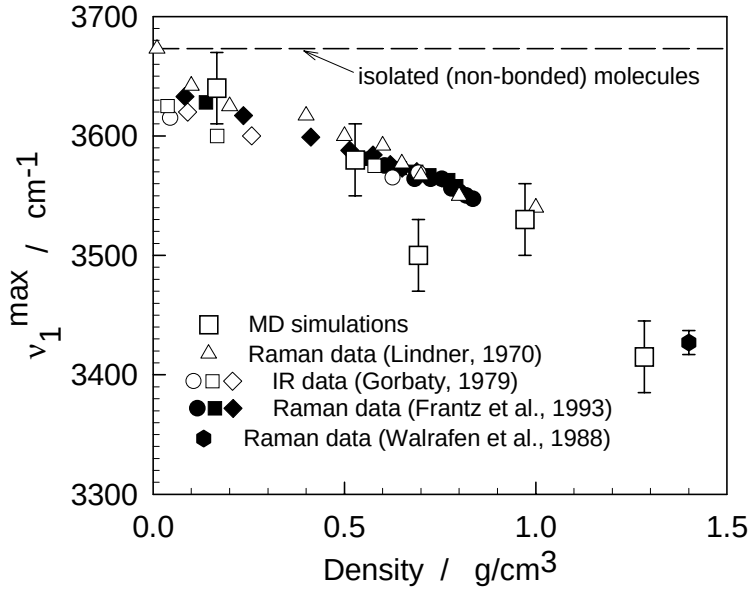

Figure 21. Spectral density maximum of the symmetric stretching vibration, ν_1^{max}, as a function of water density under supercritical conditions. Big open squares – MD simulations for the BJH model. Other symbols – experimental data from various sources.

experimental error up to 573 K. In MD simulations of high-density BJH water Jancsó et al. (1984) obtained $\nu_2 = 1729 \pm 5$ cm^{-1} at 350 K and a density of 1.346 g/cm^3, quite close to that of the run E in Table 5. Comparing these values, we see that the bending frequency remains unchanged over a wide temperature range at high densities, as well. On the other hand, the blue shift of ν_2 with increasing density at 673 K (runs A and D) and 773 K (runs B and E) is also in good agreement with Raman spectroscopic data (Farber et al. 1990; Kohl et al. 1991).

With the gas-phase harmonic vibrational frequencies for the BJH water model being $\nu_1 = 3832$ cm^{-1}, $\nu_2 = 1649$ cm^{-1}, and $\nu_3 = 3943$ cm^{-1} (Bopp et al. 1983), it is also interesting to note that at the lowest density studied (run A in Table 5) the bending frequency is already close enough to its gas-phase value, while the two stretching frequencies are still about ≈200 cm^{-1} red-shifted with respect to their corresponding gas-phase values. This clearly indicates that the stretching vibrational modes in supercritical water are much more sensitive to the changes in local molecular environment, and they are much more strongly influenced by the effects of hydrogen bonding and molecular clusterization, than the bending vibrational mode, even at relatively low vapor-like densities. High-temperature experimental data on the asymmetric stretching vibrations, ν_3, are available only over a limited range of relatively low pressures, P<50 MPa (Bondarenko and Gorbaty 1973). However, the general temperature and density dependence of our simulated spectra seem to be in qualitative agreement with these data.

The shapes of the vibrational spectra obtained from the MD simulations using the procedure described above, which employs only simple classical-mechanical considerations, can not be directly compared with the shapes of experimental Raman or infrared spectra. However, it is nevertheless instructive to analyze how the widths of the simulated spectra change with density. The width of the ν_1 stretching band increases almost linearly with the rate of ≈200 cm^{-1}/(g·cm^{-3}) over the entire density range (Table 5 and Fig. 20). This density broadening agrees surprisingly well with experimental results of Lindner (1970), from which a rate of about ≈175 cm^{-1}/(g·cm^{-3}) can be derived at a supercritical temperature of 673 K over approximately the same density range. From the Raman data of Frantz et al. (1993) a rate from 100 to 160 cm^{-1}/(g·cm^{-3}) can be estimated at temperatures between 630 and 780 K and over a somewhat narrower density range. Thus, we again see quite satisfactory agreement with experimental data.

CONCLUSIONS AND OUTLOOK

The results of numerous computer simulations in recent years have demonstrated that hydrogen bonding is still noticeable in supercritical water even at temperatures as high as 800 K and very low densities. After some controversy, these results now seem to agree well with all available experimental data from several independent sources. Obviously, more experimental diffraction and spectroscopic measurements under supercritical conditions are necessary before these structural data can be used for reliable reparameterization of the available and the development of new intermolecular potential functions used in computer simulations for specifically supercritical conditions. Some of this work is already under way (Errington and Panagiotopoulos 1998; Stern et al. 1999; Chen et al. 2000; Guillot and Guissani 2000). However, even in their present form the effective semi-empirical potentials like TIP4P, SPC, or BJH are able to qualitatively, and often even quantitatively, reproduce the structure and properties of supercritical water.

The predictive value of classical computer simulations for aqueous systems is still questioned by some researchers (Brodsky 1996). Yet, the case of the interpretation of the picture of hydrogen bonding in supercritical water clearly proves that such simulations

can yield extremely useful information, when performed and analyzed carefully. The detailed picture of hydrogen bonding in liquid and supercritical water seems to be quite adequately described by classical simulations using relatively simple empirical potentials where the only reason for intermolecular H-bonding arises due to electrostatic interactions between partially charged atoms. On the other hand, recent *ab initio* MD simulations (Tukerman et al. 1997) and experiments (Isaacs et al. 1999; Martin and Derevenda 1999) have shown that up to 10% of H-bonding interactions is due to covalent forces, at least in liquid water and ice.

Of course, the purely classical-mechanical approach to the high-frequency vibrational motions accepted here is limited by the exclusion of any quantum effects. However, these effects are expected to cancel out, if we are mainly interested in the changes of the vibrational frequencies, and not so much in their absolute values (Bopp et al. 1983). This is especially true for the supercritical conditions discussed in this chapter.

Computer simulations are sometimes used in the geochemical literature with the sole objective to predict thermodynamic *PVT* properties of molecular fluids at high temperatures and pressures (e.g., Belonoshko and Saxena 1991, 1992; Duan et al. 1992; Fraser and Refson 1992). However, the ability to improve our physical understanding of the complex chemical behavior of geochemical fluids and to unravel fundamental molecular-scale correlations between the structural, transport, spectroscopic, and thermodynamic properties of supercritical aqueous fluids, seems to be a much more important feature of these techniques.

Being an invaluable source of information intermediate between theory and experiment, the methods of molecular computer simulations will definitely continue to greatly stimulate the development of both theoretical and experimental studies of geochemical fluids in the near future. With the continuing progress in computer technology, which makes the use of powerful supercomputers less expensive and easily accessible for large-scale simulation studies by almost any geochemical laboratory, the prospects of molecular computer simulations of aqueous geochemical fluids look now more promising than ever.

ACKNOWLEDGMENTS

The author is extremely grateful to YE Gorbaty, K Heinzinger, JD Bass, SV Churakov, and RJ Kirkpatrick for many years of fruitful collaboration some results of which are presented in this chapter. The financial support of the Russian Basic Research Foundation (grants 95-05-14748 and 97-03-32587), INTAS (grants UA-95-0096 and 96-1989), CRDF (grant RC1-170 to YE Gorbaty), NSF (grant EAR-9305071 to JD Bass, and grant EAR 97-05746 to RJ Kirkpatrick), and U.S. Department of Energy (grant DEF02-00ER1528 to RJ Kirkpatrick), is most gratefully acknowledged. The computations were partly supported by the National Computational Science Alliance (grant EAR 990003N) and utilized NCSA SGI/CRAY Origin 2000 computers.

REFERENCES

Allen MP, Tildesley DJ (1987) Computer Simulation of Liquids. Oxford University Press, New York

Alper HE, Levy RM (1989) Computer simulations of the dielectric properties of water: Studies of the simple point charge and transferable intermolecular potential models. J Chem Phys 91:1242-1251

Balbuena PB, Johnson KP, Rossky PJ (1996a) Molecular dynamics simulation of electrolyte solutions in ambient and supercritical water. 1. Ion solvation. J Phys Chem 100:2706-2715

Balbuena PB, Johnson KP, Rossky PJ (1996b) Molecular dynamics simulation of electrolyte solutions in ambient and supercritical water. 2. Relative acidity of HCl. J Phys Chem 100:2716-2722

Balbuena PB, Seminario JM (eds) (1999) Molecular Dynamics: From Classical to Quantum Methods. Elsevier, Amsterdam.

Balbuena PB, Wang L, Li T, Derosa PA (1999) *Ab initio* and molecular dynamics studies of cation-water interactions. *In:* Balbuena PB, Seminario JM (eds) Molecular Dynamics: From Classical to Quantum Methods. Elsevier, Amsterdam, p 431-469

Barker JA, Watts RO (1969) Structure of water; A Monte Carlo calculation. Chem Phys Lett 3:144-145

Barnes HL (ed) (1997) Geochemistry of Hydrothermal Ore Deposits John Wiley & Sons, New York, 1997

Barrat J-L, McDonald IR (1990) The role of molecular flexibility in simulations of water. Mol Phys 70:535-539

Belch AC, Rice SA, Sceats MG (1981) A test of the random network model of water using molecular dynamics simulation data. Chem Phys Lett 77:455-459

Bellisent-Funel MC, Tassaing T, Zhao H, Beysens D, Guillot B, Guissani Y (1997) The structure of supercritical heavy water as studied by neutron diffraction. J Chem Phys 107:2942-2949

Belonoshko A, Saxena SK (1991) A molecular dynamics study of the P-V-T properties of supercritical fluids: I. H_2O. Geochim Cosmochim Acta 55:381-387

Belonoshko A, Saxena SK (1992) Equations of state of fluids at high temperature and pressure (water carbon dioxide, methane, oxygen, and hydrogen). *In:* Saxena SK (ed) Thermodynamic Data: Systematics and Estimation (Adv Phys Geochem, v.10), Springer-Verlag, New York, p 79-97

Bennett GE, Johnston KP (1994) UV-visible absorbance spectroscopy of organic probes in supercritical water. J Phys Chem 98:441-447

Berendsen HJC, Grigeira JR, Straatsma TP (1987) The missing term in effective pair potentials. J Phys Chem 91:6269-6271

Berendsen HJC, Postma JPM, Van Gunsteren WF, Hermans J (1981) Interaction models for water in relation to protein hydration. *In:* Pullman B (ed) Intermolecular Forces. Riedel, Dordrecht, p 331-342

Beshinske RJ, Lietzke MH (1969) Monte Carlo calculation of some thermodynamic properties of steam using a dipole-quadrupole potential. J Chem Phys 51:2278-2279

Blumberg RL, Stanley HE, Geiger A, Mausbach P (1984) Connectivity of hydrogen bonds in liquid water. J Chem Phys 80:5230-5241

Bondarenko GV, Gorbaty YE (1973) ν_3 infrared spectra of HDO at high pressures and temperatures, Doklady Physical Chemistry 210:369-371

Bondarenko GB, Gorbaty YE (1991) An IR study of water vapor in the temperature range 573-723K. Dimerization enthalpy and absorption intensities for monomer and dimer. Mol Phys 74:639-647

Bondarenko GB, Gorbaty YE (1997) *In situ* Raman spectroscopic study of sulfur-saturated water at 1000 bar between 200 and 500°C. Geochim Cosmochim Acta 61:1413-1420

Bopp P (1986) A study of the vibrational motions of water in an aqueous $CaCl_2$ solution. Chem Phys 106:205-212

Bopp P (1987) Molecular dynamics computer simulations of solvation in hydrogen bonded systems. Pure & Appl Chem 59:1071-1082

Bopp P, Jancsó G, Heinzinger K (1983) An improved potential for non-rigid water molecules in the liquid phase. Chem Phys Lett 98:129-133

Botti A, Bruni F, Ricci MA, Soper AK (1998) Neutron diffraction study of high density supercritical water. J Chem Phys 109:3180-3184

Brodholt JP (1998) Molecular dynamics simulations of aqueous NaCl solutions at high pressures and temperatures. Chem Geology 151:11-19

Brodholt JP, Wood BJ (1990) Molecular dynamics of water at high temperatures and pressures. Geochim Cosmochim Acta 54:2611-2616

Brodholt JP, Wood BJ (1993a) Simulations of the structure and thermodynamic properties of water at high temperatures and pressures. J Geophys Res 98B:519-536

Brodholt JP, Wood BJ (1993b) Molecular dynamics simulations of the properties of CO_2-H_2O mixtures at high pressures and temperatures. Amer Mineralogist 78:558-564

Brodsky A (1996) Is there predictive value in water computer simulations? Chem Phys Lett 261:563-568

Bruni F, Ricci MA, Soper AK (1996) Unpredicted density dependence of hydrogen bonding in water found by neutron diffraction. Phys Rev B 54:11876-11879

Carney GD, Curtiss LA, Langhoff SR (1976) Improved potential functions for bent AB_2 molecules: water and ozone. J Mol Spectr 61:371-379

Carravetta V, Clementi E (1984) Water-water interaction potential: An approximation of electron correlation contribution by a functional of the SCF density matrix. J Chem Phys 81:2646-2651

Chen B, Xing J, Siepman JI (2000) Development of polarizable water force fields for phase equilibrium calculations. J Phys Chem B, 104:2391-2400

Chialvo AA, Cummings PT (1994) Hydrogen bonding in supercritical water. J Chem Phys 101:4466-4469

Chialvo AA, Cummings PT (1996) Microstructure of ambient and supercritical water. Direct comparison between simulation and neutron scattering experiments. J Phys Chem 100:1309-1316

Chialvo AA, Cummings PT (1999) Molecular-based modeling of water and aqueous solutions at supercritical conditions. Adv Chem Phys 109:115-205

Chialvo AA, Cummings PT, Simonson JM, Mesmer RE, Cochran HD (1998) Interplay between molecular simulation and neutron scattering in developing new insights into the structure of water. Ind Eng Chem Res 37:3021-3025

Chialvo AA, Yezdimer E, Driesner T, Cummings PT, Simonson JM (2000) The structure of water from 25^{o}C to 457^{o}C: Comparison between neutron scattering and molecular simulation. Chem Phys 258:109-120

Churakov SV, Kalinichev AG (2000) Size, structure and abundance of molecular clusters in supercritical water over a wide range of densities: Monte Carlo simulations. *In:* Tremaine PR, Hill PG, Irish DE, Balakrishnan PV (eds) Steam, Water, and Hydrothermal Systems: Physics and Chemistry Meeting the Needs of Industry. NRC Press, Ottawa, p 418-425

Clementi E (1985) *Ab initio* computational chemistry. J Phys Chem 89:4426-4436

Corongiu G (1992) Molecular dynamics simulation for liquid water using a polarizable and flexible potential. Int J Quantum Chem 42:1209-1235

Cui ST, Harris JG (1994) Ion association and liquid structure in supercritical water solutions of sodium chloride: A microscopic view from molecular dynamics simulations. Chem Eng Sci 49:2749-2763

Cui ST, Harris JG (1995) Solubility of sodium chloride in supercritical water: A molecular dynamics study. J Phys Chem 99:2900-2906

Cummings PT, Cochran HD, Simonson JM, Mesmer RE, Karaborni S (1991) Simulation of supercritical water and of supercritical aqueous solutions. J Chem Phys 94:5606-5621

Dang LX, Pettitt BM (1987) Simple intermolecular model potentials for water. J Phys Chem 91:3349-3354

De Jong PHK, Neilson GW (1997) Hydrogen-bond structure in an aqueous solution of sodium chloride at sub- and supercritical conditions. J Chem Phys 107:8577-8585

De Pablo JJ, Prausnitz JM (1989) Phase equilibria for fluid mixtures from Monte Carlo simulation. Fluid Phase Equil 53:177-189

De Pablo JJ, Prausnitz JM, Strauch HJ, Cummings PT (1990) Molecular simulation of water along the liquid-vapor coexistence curve from 25°C to the critical point. J Chem Phys 93:7355-7359

Destrigneville CM, Brodholt JP, Wood BJ (1996) Monte Carlo simulation of H_2O-CO_2 mixtures to 1073.15 K and 30 kbar. Chem Geology 133:53-65

Driesner T (1997) The effect of pressure on deuterium-hydrogen fractionation in high-temperature water. Science 277:791-794

Driesner T, Cummings PT (1999) Molecular simulation of the temperature and density dependence of ionic hydration in aqueous $SrCl_2$ solutions using rigid and flexible water models. J Chem Phys 111:5141-5149

Driesner T, Seward TM (2000) Experimental and simulation study of salt effects and pressure/density effects on oxygen and hydrogen stable isotope liquid-vapor fractionation for 4-5 molal aqueous NaCl and KCl solutions to 300^{o}C. Geochim Cosmochim Acta 64:1773-1784

Driesner T, Seward TM, Tironi IG (1998) Molecular dynamics simulation study of ionic hydration and ion association in dilute and 1 molal aqueous sodium chloride solutions from ambient to supercritical conditions. Geochim Cosmochim Acta 62:3095-3107

Duan Z, Møller N, Weare JH (1992) Molecular dynamics simulation of PVT properties of geological fluids and a general equation of state on nonpolar and weakly polar gases up to 2000 K and 20,000 bar. Geochim Cosmochim Acta 56:3839-3845

Duan Z, Møller N, Weare JH (1995) Molecular dynamics simulation of water properties using RWK2 potential – from clusters to bulk water. Geochim Cosmochim Acta 59:3273-3283

Eisenberg D, Kauzmann W (1969) The Structure and Properties of Water. Oxford University Press, Oxford

Errington JR, Panagiotopoulos AZ (1998) Phase equilibria of the modified Buckingham exp-6 potential from Hamiltonian scaling grand canonical Monte Carlo. J Chem Phys 109:1093-1100

Eugster HP, Baumgartner L (1987) Mineral solubilities and speciation in supercritical metamorphic fluids. *In:* Carmichael ISE, Eugster HP (eds) Thermodynamic Modeling of Geological Materials: Minerals, Fluids and Melts. (Reviews in Mineralogy, v.17), Mineralogical Society of America, Washington, D.C., p 367-403

Evans MW (1986) Molecular dynamical simulation of new auto and cross correlations in liquid water. J Mol Liquids 32:173-181

Evans MW, Lie GC, Clementi E (1988) Molecular dynamics simulation of water from 10 to 1273 K. J Chem Phys 88:5157-5165

Falk M (1990) Frequencies of H-O-H, H-O-D and D-O-D bending fundamentals in liquid water. J Raman Spectrosc., 21:563-567

Famulari A, Specchio R, Sironi M, Raimondi M (1998) New basis set superposition error free *ab initio* MO-VB interaction potential: Molecular dynamics simulation of water at critical and supercritical conditions. J Chem Phys 108:3296-3303

Farber DL, Williams Q, Knittle E (1990) Raman spectra of liquid water at high pressures and temperatures. EOS Trans Amer Geophys Union 71:1600

Floris FM, Tani A (1999) Interaction potentials for small molecules. *In:* Balbuena PB, Seminario JM (eds) Molecular Dynamics: From Classical to Quantum Methods. Elsevier, Amsterdam, p 363-429

Fois ES, Sprik M, Parrinello M (1994) Properties of supercritical water - an *ab initio* simulation. Chem Phys Lett 223:411-415

Franck EU, Roth K (1967) Infrared absorption of HDO in water at high pressures and temperatures. Disc Farad Soc 43:108-114

Frantz JD, Dubessy J, Mysen B (1993) An optical cell for Raman spectroscopic studies of supercritical fluids and its application to the study of water to 500°C and 2000 bar. Chem Geol 106:9-26

Fraser DG, Refson K (1992) Estimating thermodynamic properties by molecular dynamics simulations: The properties of fluids at high pressures and temperatures.. *In:* Saxena SK (ed) Thermodynamic Data: Systematics and Estimation (Adv Phys Geochem, v.10), Springer-Verlag, New York, p 60-78

Frenkel D, Smit B (1996) Understanding molecular simulation: From algorithms to applications. Academic Press, San Diego

Gao J (1994) Simulation of the Na^+Cl^- ion pair in supercritical water. J Phys Chem 98:6049-6053

Gellatly BJ, Quinn JE, Barnes P, Finney JL (1983) Two, three, and four body interactions in model water interactions. Mol Phys 59:949-970

Gil-Adalid L, Ortega-Blake I (1991) Four-body nonadditivity in liquid water. J Chem Phys 94:3748-3752

Gorbaty YE (1979) Some new data on the structure and properties of liquid and supercritical water. *In:* Problems of Physical-Chemical Petrology, v.II, Nauka, Moscow, p 15-24 (in Russian)

Gorbaty YE, Bondarenko GV, Kalinichev AG, Okhulkov AV (1999) The effect of pressure on hydrogen bonding in water: IR study of ν_{OD} HDO at pressures of up to 1500 bar. Mol Phys, 96:1659-1665

Gorbaty YE, Demianets YN (1983) The pair correlation functions of water at a pressure of 1000 bar in the temperature range 25-500°C. Chem Phys Lett 100:450-455

Gorbaty YE, Gupta RB (1998) The structural features of liquid and supercritical water. Ind Eng Chem Res 37:3026-3035

Gorbaty YE, Kalinichev AG (1995) Hydrogen bonding in supercritical water. 1. Experimental results. J Phys Chem 99:5336-5340

Guillot B, Guissani Y (2000) An accurate pair potential for simulated water. *In:* Tremaine PR, Hill PG, Irish DE, Balakrishnan PV (eds) Steam, Water, and Hydrothermal Systems: Physics and Chemistry Meeting the Needs of Industry. NRC Press, Ottawa, p 562-570

Guissani Y, Guillot B (1993) A computer simulation study of the liquid-vapor coexistence curve of water. J Chem Phys 98:8221-8235

Guissani Y, Guillot B, Bratos S (1988) The statistical mechanics of the ionic equilibrium in water: A computer simulation study. J Chem Phys 88:5850-5856

Gupta RB, Panayiotou CG, Sanchez IC, Johnston KP (1992) Theory of hydrogen bonding in supercritical fluids. AIChE Journal 38:1243-1253

Halley JW, Rustad JR, Rahman A (1993) A polarizable, dissociating molecular dynamics model for liquid water. J Chem Phys 98:4110-4119

Hansen JP, McDonald IR (1986) Theory of Simple Liquids. (2nd Ed.) Academic Press, London

Heinzinger K (1986) MD simulations of the effect of pressure on the structural and dynamical properties of water and aqueous electrolyte solutions. *In:* Dupuis M (ed) Supercomputer Simulations in Chemistry, (Lecture Notes in Chemistry, v.44), Springer-Verlag, Berlin, p 261-279

Heinzinger K (1990) Molecular dynamics simulation of aqueous systems. *In:* Computer Modelling of Fluids, Polymers and Solids. Edited by C.R.A.Catlow et al., Kluwer Academic Publishers, Dordrecht, p 357-394

Heinzinger K, Vogel PC (1976) A molecular dynamics study of aqueous solutions. III. A comparison of selected alkali halides. Z Naturforsch 31a:463-475

Helgeson HC (1979) Mass transfer among minerals and hydrothermal solutions. *In:* Barnes HL (ed) Geochemistry of Hydrothermal Ore Deposits, 2nd ed. John Wiley & Sons, New York

Helgeson HC (1981) Prediction of the thermodynamic properties of electrolytes at high pressures and temperatures. *In:* Rickard DT, Wickman FE (eds) Chemistry and Geochemistry of Solutions at High Temperatures and Pressures. Pergamon Press, Oxford, p 133-177

Hoffmann MM, Conradi MS (1997) Are there hydrogen bonds in supercritical water? J Am Chem Soc 119:3811-3817

Horita J, Driesner T, Cole DR (1999) Pressure effect on hydrogen isotope fractionation between brucite and water at elevated temperatures. Science 286:1545-1547

Hu SM, Zhang RH, Zhang XT (2000) A study of near- and super-critical fluids using diamond anvil cell and *in situ* FT-IR spectroscopy Acta Geologica Sinica-English Edition 74:412-417

Impey RW, Klein ML, McDonald IR (1981) Molecular dynamics study of the structure of water at high temperatures and density. J Chem Phys 74:647-652

Isaacs ED, Shukla A, Platzman PM, Hamann DR, Barbiellini B, Tulk CA (1999) Covalency of the hydrogen bond in ice: A direct X-ray measurement. Phys Rev ett 82:600-603

Jancsó G, Bopp P, Heinzinger K (1984) Molecular dynamics study of high-density liquid water using a modified central-force potential. Chem Phys 85:377-387

Jedlovszky P, Brodholt JP, Bruni F, Ricci MA, Soper AK, Vallauri R (1998) Analysis of the hydrogen-bonded structure of water from ambient to supercritical conditions. J Chem Phys 108:8528-8540

Jedlovszky P, Richardi J (1999) Comparison of different water models from ambient ot supercritical conditions: A Monte Carlo simulation and molecular Ornstein_Zernike study. J Chem Phys 110:8019-8031

Jedlovszky P, Vallauri R, Richardi J (2000) The change of the structural and thermodynamic properties of water from ambient to supercritical conditions as seen by computer simulations. J Phys Cond Matter 12:A115-A122

Jorgensen WL, Chandrasekhar J, Madura JD, Impey RW, Klein ML (1983) Comparison of simple potential functions for simulating liquid water. J Chem Phys 79:926-935

Jorgensen WL, Jenson C (1998) Temperature dependence of TIP3P, SPC, and TIP4P water from NPT Monte Carlo simulations: Seeking temperatures of Maximum density. J Comput Chem 19:1179-1186

Jorgensen WL, Madura JD (1985) Temperature and size dependence for Monte Carlo simulations of TIP4P water. Mol Phys 56:1381-1392

Jupp T, Schultz A (2000) A thermodynamic explanation for black smoker temperatures. Nature 403:880-883

Kalinichev AG (1985) A Monte Carlo study of dense supercritical water. High Temperature 23:544-548

Kalinichev AG (1986) Monte Carlo study of the thermodynamics and structure of dense supercritical water. Intern J Thermophys 7:887-900

Kalinichev AG (1991) Monte Carlo simulations of water under supercritical conditions. I. Thermodynamic and structural properties. Z Naturforsch 46a:433-444

Kalinichev AG (1992) Monte Carlo simulations of water under supercritical conditions. II. Convergence characteristics and the system size effects. Z Naturforsch 47a:992-998

Kalinichev AG (1993) Molecular dynamics and self-diffusion in supercritical water. Ber Bunsenges Phys Chem 97:872-876

Kalinichev AG, Bass JD (1994) Hydrogen bonding in supercritical water: a Monte Carlo simulation. Chem Phys Lett 231:301-307

Kalinichev AG, Bass JD (1995) Computer simulations of supercritical water over a wide range of densities. *In:* White HJ Jr, Sengers JV, Neumann DB, Bellows JC (eds) Physical Chemistry of Aqueous Systems: Meeting the Needs of Industry. Begell House, New York, p 245-252

Kalinichev AG, Bass JD (1997) Hydrogen bonding in supercritical water. 2. Computer simulations. J Phys Chem A 101:9720-9727

Kalinichev AG, Churakov SV (1999) Size and topology of molecular clusters in supercritical water: A molecular dynamics simulation. Chem Phys Lett 302:411-417

Kalinichev AG, Gorbaty YE (1998) The role of hydrogen bonding in the structure and properties of hydrothermal fluids. *In:* Zharikov VA (ed) Experimental and Theoretical Modeling of Mineral Formation Processes. Moscow, Nauka, p 242-264 (in Russian)

Kalinichev AG, Gorbaty YE, Okhulkov AV (1999) Structure and hydrogen bonding of liquid water at high hydrostatic pressures: Monte Carlo NPT-ensemble simulation up to 10 kbar. J Mol Liquids 82:57-72

Kalinichev AG, Heinzinger K (1992) Computer simulations of aqueous fluids at high temperatures and pressures. *In:* Saxena SK (ed) Thermodynamic Data: Systematics and Estimation (Adv Phys Geochem, v.10), Springer-Verlag, New York, p 1-59

Kalinichev AG, Heinzinger K (1995) Molecular dynamics of supercritical water: A computer simulation of vibrational spectra with the flexible BJH potential. Geochim Cosmochim Acta 59:641-650

Karim OA, Haymet AD (1988) The ice/water interface: A molecular dynamics simulation study. J Chem Phys 89:6889-6896

Kataoka Y (1987) Studies of liquid water by computer simulations. V. Equation of state of fluid water with Carravetta-Clementi potential. J Chem Phys 87:589-598

Kataoka Y (1989) Studies of liquid water by computer simulations. VI. Transport properties of Carravetta-Clementi water. Bull Chem Soc Jpn 62:1421-1431

Kiyohara K, Gubbins KE, Panagiotopoulos AZ (1998) Phase coexistence properties of polarizable water models. Mol Phys 94:803-808

Klug DD, Whalley E (1984) The pressure dependence of the infrared spectrum of HDO in D_2O to 189 kbar. Mat Res Soc Symp Proc 22, pt III, p 315-318

Kohl W, Lindner HA, Franck EU (1991) Raman spectra of water to 400°C and 3000 bar. Ber Bunsenges Phys Chem 95:1586-1593

Lamb WJ, Hoffman GA, Jonas J (1981) Self-diffusion in compressed supercritical water. J Chem Phys 74:6875-6880

Landau LD, Lifshitz EM (1980) Statistical Physics. Pergamon Press, Oxford.

La Placa SJ, Hamilton WC, Kamb B, Prakash A (1973) On a nearly proton-ordered structure for ice IX. J Chem Phys 58:567-580

Levelt-Sengers JMH (1990) Thermodynamic properties of aqueous solutions at high temperatures: Needs, methods, and challenges. Int J Thermophys 11:399-415

Lie GC, Clementi E (1986) Molecular-dynamics simulation of liquid water with an *ab initio* flexible water-water interaction potential. Phys Rev A 33:2679-2693

Liew CC, Inomata H, Arai K, Saito S (1998) Three-dimensional structure and hydrogen bonding of water in sub- and supercritical regions: a molecular simulation study. J Supercrit Fluids 13:83-91

Lin CL, Wood RH (1996) Prediction of the free energy of dilute aqueous methane, ethane, and propane at temperatures from 600 to 1200°C and densities from 0 to 1 g/cm^3 using molecular dynamics simulations. J Phys Chem 100:16339-16409

Lindner HA (1970) Ramanspektroskopische Untersuchungen an HDO, gelöst in H_2O, an HDO in wässrigen Kaliumjodidlösungen und an reinem H_2O bis 400°C und 5000 bar. PhD Thesis, Karlsruhe.

Löffler G, Schreiber H, Steinhauser O (1994) Computer simulation as a tool to analyze neutron scattering experiments: Water at supercritical temperatures. Ber Bunsenges Phys Chem 98:1575-1578

Lu T, Tóth G, Heinzinger K (1996) Systematic study of the spectroscopic properties of isotopically substituted water by MD simulations. J Phys Chem 100:1336-1339

Luck W (1965) Association of water. III. Temperature dependence of the water IR bands up to the critical point. Ber Bunsenges Phys Chem 69:627-637

Lynch GC, Pettitt BM (1997) Grand canonical ensemble molecular dynamics simulations: Reformulation of extended system dynamics approaches. J Chem Phys 107:8594-8610

Madura JD, Pettitt BM, Calef DF (1988) Water under high pressure. Mol Phys 64:325

Mahoney MW, Jorgensen WL (2000) A five-site model for liquid water and the reproduction of the density anomaly by rigid, nonpolarizable potential functions. J Chem Phys 112:8910-8922

Marchi RP, Eyring H (1964) Application of significant structure theory to water. J Phys Chem 68:221-228

Martin MG, Chen B, Siepman JI (1998) A novel Monte Carlo algorithm for polarizable force fields. Application to a fluctuating charge model for water. J Chem Phys 108:3383-3385

Martin TW, Derewenda ZS (1999) The name is bond — H bond. Nature Struct Biology 6:403-406

Matsuoka O, Clementi E, Yoshimine M (1976) CI study of the water dimer potential surface. J Chem Phys 64:1351-1361

Matubayasi N, Wakai C, Nakahara M (1997a) NMR study of water structure in super- and subcritical conditions. Phys Rev Lett 78:2573-2576

Matubayasi N, Wakai C, Nakahara M (1997b) Structural study of supercritical water. I. NMR spectroscopy. J Chem Phys 107:9133-9140

Matubayasi N, Wakai C, Nakahara M (1999) Structural study of supercritical water. II. Computer simulations. J Chem Phys 110:8000-8011

McQuarrie DA (1976) Statistical Mechanics, Harper & Row, New York

Mezei M, Beveridge DL (1981) Theoretical studies of hydrogen bonds in liquid water and dilute aqueous solutions. J Chem Phys 74:622-630

Mills MF, Reimers JR, Watts RO (1986) Monte Carlo simulation of the OH stretching spectrum of solutions of KCl, KF, LiCl and LiF in water. Mol Phys 57:777-791.

Mizan TI, Savage PE, Ziff RM (1994) Molecular dynamics of supercritical water using a flexible SPC model. J Phys Chem 98:13067-13076

Mizan TI, Savage PE, Ziff RM (1996) Temperature dependence of hydrogen bonding in supercritical water. J Phys Chem 100:403-408

Molecular Simulations Inc. (1999) Cerius2-4.0 User Guide. Forcefield-Based Simulations. MSI, San Diego.

Morse MD, Rice SA (1982) Tests of effective pair potentials for water: Predicted ice structures. J Chem Phys 76:650-660

Motakabbir KA, Berkowitz ML (1991) Liquid-vapor interface of TIP4P water: comparison between a polarizable and a nonpolarizable model. Chem Phys Lett 176:61-66

Mountain RD (1989) Molecular dynamics investigation of expanded water at elevated temperatures. J Chem Phys 90:1866-1870

Mountain RD (1995) Comparison of a fixed-charge and polarizable water model. J Chem Phys 101:3084-3090

Mountain RD (1999) Voids and clusters in expanded water. J Chem Phys 110:2109-2115

Neumann M (1986) Dielectric relaxation in water. Computer simulations with the TIP4P potential. J Chem Phys 85:1567-1580

Norton DL (1984) Theory of hydrothermal systems. Annu Rev Earth Planet Sci 12:155-177

Okhulkov AV, Demianets YN, Gorbaty YE (1994) X-ray scattering in liquid water at pressures up to 7.7 kbar: Test of a fluctuation model. J Chem Phys 100:1578-1587

O'Shea SF, Tremaine PR (1980) Thermodynamics of liquid and supercritical water to 900^{o}C by a Monte Carlo method. J Phys Chem 84:3304-3306

Pálinkás G, Bopp P, Jancsó G, Heinzinger K (1984) The effect of pressure on the hydrogen bond structure of liquid water. Z Naturforsch 39a:179-185

Panagiotopoulos AZ (1987) Direct determination of phase coexistence properties of fluids by Monte Carlo simulation in a new ensemble. Mol Phys 61:813-826.

Panagiotopoulos AZ (2000) Force field development for simulations of condensed phases. *In:* Proceedings of FOMMS-2000. First International Conference on Foundations of Molecular Modeling and Simulations, (in print).

Planetary Fluids, Special issue (1990) Science 248:281-345

Postorino P, Tromp RH, Ricci MA, Soper AK, Neilson GW (1993) The interatomic structure of water at supercritical temperatures. Nature 366:668-671

Rahman A, Stillinger FH (1971) Molecular dynamics study of liquid water. J Chem Phys 55:3336-3359

Rapaport DC (1983) Hydrogen bonds in water. Network organization and lifetimes. Mol Phys 50:1151-1162

Ratcliffe CI, Irish DE (1982) Vibrational spectral studies of solutions at elevated temperatures and pressures. 5. Raman studies of liquid water up to 300°C. J Phys Chem 86:4897-4905

Re M, Laria D (1997) Dynamics of solvation in supercritical water. J Phys Chem B 101:10494-10505

Reagan M, Harris JG, Tester JW (1999) Molecular simulations of dense hydrothermal NaCl-H_2O solutions from subcritical to supercritical conditions. J Phys Chem B 103:7935-7941

Ree FH (1982) Molecular interaction of dense water at high temperature. J Chem Phys 76:6287-6302

Reimers JR, Watts RO, Klein ML (1982) Intermolecular potential functions and the properties of water. Chem Phys 64:95-114

Robinson GW, Zhu SB, Singh S, Evans MW (1996) Water in Biology, Chemistry and Physics. World Scientific, Singapore.

Ruff I, Diestler DJ (1990) Isothermal-isobaric molecular dynamics simulation of liquid water. J Chem Phys 93:2032-2042

Saul A, Wagner W (1989) A fundamental equation for water covering the range from the melting line to 1273 K at pressures up to 25000 MPa. J Phys Chem Ref Data 18:1537-1564

Seward TM, Barnes HL (1997) Metal transport by hydrothermal ore fluids. *In:* Barnes HL (ed) Geochemistry of Hydrothermal Ore Deposits. John Wiley & Sons, New York, p 435-486

Seward TM, Henderson CMB, Charnock JM, Driesner T (1999) An EXAFS study of solvation and ion pairing in aqueous strontium solutions to 300^{o}C. Geochim Cosmochim Acta 63:2409-2418

Shaw RW, Brill TB, Clifford AA, Eckert CA, Franck EU (1991) Supercritical water: A medium for chemistry. Chem & Eng News, 69:26-39

Shelley JC, Patey GN (1995) A configuration bias Monte-Carlo method for water. J Chem Phys 102:7656-7663

Shroll RM, Smith DE (1999a) Molecular dynamics simulations in the grand canonical ensemble: Formulation of a bias potential for umbrella sampling. J Chem Phys 110:8295-8302

Shroll RM, Smith DE (1999b) Molecular dynamics simulations in the grand canonical ensemble: Application to clay mineral swelling. J Chem Phys 111:9025-9033

Smith DE, Haymet ADJ (1992) Structure and dynamics of water and aqueous solutions: The role of flexibility. J Chem Phys 96:8450-8459

Smits PJ, Economou IG, Peters CJ, de Swan Arons J (1994) Equation of state description of thermodynamic properties of near-critical and supercritical water. J Phys Chem 98:12080-12085

Soper AK (1996) Bridge over troubled water: the apparent discrepancy between simulated and experimental non-ambient water structure. J Phys Condens Matter 8:9263-9267

Soper AK, Bruni F, Ricci MA (1997) Site-site pair correlation functions of water from 25 to 400°C. Revised analysis of new and old diffraction data. J Chem Phys 106:247-254

Spohr E, Pálinkás G, Heinzinger K, Bopp P, Probst MM (1988) Molecular dynamics study of an aqueous $SrCl_2$ solution. J Phys Chem 92:6754-6761

Stern HA, Kaminski GA,Banks JL, Zhou R, Berne BJ, Friesner RA (1999) Fluctuating charge, polarizable dipole, and combined models: Parameterization from *ab initio* quantum chemistry. J Phys Chem B 103:4730-4737

Stillinger FH (1980) Water revisited. Science 209:451-457

Stillinger FH, Rahman A (1972) Molecular dynamics study of temperature effects on water structure and kinetics. J Chem Phys 57:1281-1292

Stillinger FH, Rahman A (1974a) Improved simulation of liquid water by molecular dynamics. J Chem Phys 60:1545-1557.

Stillinger FH, Rahman A (1974b) Molecular dynamics study of liquid water under high compression. J Chem Phys 61:4973-4980

Stillinger FH, Rahman A (1978) Revised central force potentials for water. J Chem Phys 68:666-670

Sverjensky DA (1987) Calculation of the thermodynamic properties of aqueous species and the solubilities of minerals in supercritical electrolyte solutions. *In:* Carmichael ISE, Eugster HP (eds) Thermodynamic Modeling of Geological Materials: Minerals, Fluids and Melts. (Reviews in. Mineralogy, v.17), Mineralogical Society of America, Washington, D.C., p 177-209

Szász GI, Heinzinger K (1983a) Hydration shell structures in LiI solution at elevated temperature and pressure: a molecular dynamics study. Earth Planet. Sci. Lett. 64:163-167.

Szász GI, Heinzinger K (1983b) A molecular dynamics study of the translational and rotational motions in an aqueousLiI solution. J. Chem. Phys. 79:3467-3473.

Tanaka H, Ohmine I (1987) Large local energy fluctuations in water. J Chem Phys 87:6128-6139

Tassaing T, Bellisent-Funel MC, Guillot B, Guissani Y (1998) The partial pair correlation functions of dense supercritical water. Europhys Lett 42:265-270

Tassaing T, Bellissent-Funel MC (2000) The dynamics of supercritical water: A quasielastic incoherent neutron scattering study J Chem Phys 113:3332-3337

Teleman O, Jönsson B, Engström S (1987) A molecular dynamics simulation of a water model with intramolecular degrees of freedom. Mol Phys 60:193-203

Tester JW, Holgate HR, Armellini FJ, Webley PA, Killiea WR., Hong GT, Barner HE (1993) Supercritical water oxidation technology. *In:* Emerging Technologies in Hazardous Waste Management III, ACS Symp. Series, 518, p 35-76

Tivey MK, Olson LO, Miller VW Light RD (1990) Temperature measurements during initiation and growth of a black smoker chimney. Nature 346:51-53

Toukan K, Rahman A (1985) Molecular-dynamics study of atomic motions in water. Phys Rev B 31:2643-2648

Trokhymchuk AD, Holovko MF, Heinzinger K (1993) Static dielectric properties of a flexible water model. J Chem Phys 99:2964-2971

Tukerman M, Laasonen K, Sprik M, Parrinello M (1995) *Ab initio* molecular dynamics of the solvation and transport of H_3O^+ and OH^- ions in water. J Phys Chem 99:5749-5752

Tukerman M, Marx D, Klein M, Parrinello M (1997) On the quantum nature of the shared proton in hydrogen bonds Science 275:817-820

Uffindell CH, Kolesnikov AI, Li JC, Mayers J (2000) Inelastic neutron scattering study of water in the subcritical and supercritical region. Phys Rev B 62:5492-5495

Ugdale JM, Alkorta I, Elguero J (2000) Water clusters: Towards an understanding based on first principles of their static and dynamic properties. Angew Chem Int Ed 39:717-721

Van der Spoel D, Van Maaren PJ, Berendsen HJC (1998) A systematic study of water models for molecular simulation: Derivation of water models optimized for use with a reaction field. J Chem Phys 108:10220-10230

Vlot MJ, Huinink J, van der Eerden JP (1999) Free energy calculations on systems of rigid molecules: An application to the TIP4P model of H_2O. J Chem Phys 110:55-61

Von Damm KL (1990) Seafloor hydrothermal activity: Black smoker chemistry and chimneys. Annu Rev Earth Planet Sci 18:173-204

Wallqvist A, Mountain RD (1999) Molecular models of water: Derivation and description. *In:* Lipkowitz KB, Boyd DB (eds) Reviews in Computational Chemistry, v.13. John Wiley and Sons, New York, p 183-247.

Wallqvist A, Teleman O (1991) Properties of flexible water models. Mol Phys 74:515-533

Walrafen GE (1973) Raman spectra from partially deuterated water and ice-VI to 10.1 kbar at 28°C. J Sol Chem 2:159-171

Walrafen GE, Hokmabadi MS, Yang WH, Piermarini GJ (1988) High-temperature high-pressure Raman spectra from liquid water. J Phys Chem 92:4540-4542

Walrafen GE, Chu YC (1995) Linearity between structural correlation length and correlated-proton Raman intensity from amorphous ice and supercooled water up to dense supercritical steam. J Phys Chem 99:11225-11229

Wasserman E, Wood B, Brodholt J (1995) The static dielectric constant of water at pressures up to 20 kbar and temperatures to 1273 K: Experiment, simulations, and empirical equations. Geochim Cosmochim Acta 59:1-6

Woolley HW (1980) Thermodynamic properties for H_2O in the ideal gas state. *In:* Straub J, Scheffler K (eds) Water and Steam. Pergamon Press, Oxford, p 166-175

Yamanaka K, Yamaguchi T, Wakita H (1994) Structure of water in the liquid and supercritical states by rapid x-ray diffractometry using an imading plate detector. J Chem Phys 101:9830-9836

Yao M, Okada K (1998) Dynamics in supercritical fluid water (1998) J Phys Condens Matter 10:11459-11468

Yoshii N, Yoshie H, Miura S, Okazaki S (1998) A molecular dynamics study of sub- and supercritical water using a polarizable potential model. J Chem Phys 109:4873-4884

Zhu SB, Singh S, Robinson GW (1991) A new flexible/polarizable water model. J Chem Phys 95:2791-2799